

1 **Spatial regression analysis on 32 years total column ozone data**

2

3 J. S. Knibbe^{1,2,*}, R. J. van der A¹ and A. T. J. de Laat¹

4

5 [1]{Royal Netherlands Meteorological Institute, De Bilt, the Netherlands}

6 [2]{Faculty of Earth and Life Sciences, VU University Amsterdam}

7 *corresponding author.

8 j.s.knibbe@vu.nl

9 **Abstract.**

10

11 Multiple-regressions analysis have been performed on 32 years of total ozone column data that
12 was spatially gridded with a 1×1.5 degree resolution. The total ozone data consists of the MSR
13 (Multi Sensor Reanalysis; 1979-2008) and two years of assimilated SCIAMACHY ozone data
14 (2009-2010). The two-dimensionality in this data-set allows us to perform the regressions locally
15 and investigate spatial patterns of regression coefficients and their explanatory power. Seasonal
16 dependencies of ozone on regressors are included in the analysis.

17 A new physically oriented model is developed to parameterize stratospheric ozone. Ozone
18 variations on non-seasonal timescales are parameterized by explanatory variables describing the
19 solar cycle, stratospheric aerosols, the quasi-biennial oscillation (QBO), El Nino (ENSO) and
20 stratospheric alternative halogens (EESC). For several explanatory variables, seasonally adjusted
21 versions of these explanatory variables are constructed to account for the difference in their effect
22 on ozone throughout the year. To account for seasonal variation in ozone, explanatory variables
23 describing the polar vortex, geopotential height, potential vorticity and average day length are
24 included. Results of this regression model are compared to that of a similar analysis based on a
25 more commonly applied statistically oriented model.

26 The physically oriented model provides spatial patterns in the regression results for each
27 explanatory variable. The EESC has a significant depleting effect on ozone at high and mid-
28 latitudes, the solar cycle affects ozone positively mostly at the Southern Hemisphere, stratospheric
29 aerosols affect ozone negatively at high Northern latitudes, the effect of QBO is positive and
30 negative at the tropics and mid to high-latitudes respectively and ENSO affects ozone negatively
31 between 30°N and 30°S , particularly at the Pacific. The contribution of explanatory variables

32 describing seasonal ozone variation is generally large at mid to high latitudes. We observe ozone
33 increases with potential vorticity and day length, ozone decreases with geopotential height and
34 variable ozone effects due to the polar vortex at regions to the north and south of the polar
35 vortices.

36 Recovery of ozone is identified globally. However, recovery rates and uncertainties
37 strongly depend on choices that can be made in defining the explanatory variables. Application of
38 several trend models, each with their own pros and cons, yields a large range of recovery rate
39 estimates. Overall these results suggest that care has to be taken in determining ozone recovery
40 rates, in particular for the Antarctic ozone hole.

41

42 **1. Introduction**

43

44 The observation of an ozone hole over Antarctica during Austral spring of 1985 was an
45 important milestone for the acceptance that halogens could lead to strong regional stratospheric
46 ozone depletion (Farman et al., 1985). The role of halogens in decreasing amounts of stratospheric
47 ozone was later identified for other regions such as the Arctic (Newman et al., 1997). The most
48 important halogens leading to the decrease in ozone are chlorofluorocarbons (CFCs),
49 hydrobromofluorocarbons (HBFCs) and hydrochlorofluorocarbons (HCFCs) (Stolarski and
50 Cicerone, 1974; Molina et al., 1974; Newman et al., 2007; WMO, 2010). Political action was
51 taken to ban emissions of these gasses in the Montreal protocol in 1987 and subsequent
52 amendments. Since then, considerable research efforts have been put in monitoring the amount of
53 stratospheric ozone and investigating the chemical and dynamical variables that affect ozone. In
54 the last decade, several papers have attempted to quantify from observations the different phases of
55 the recovery of the ozone layer (e.g. Weatherhead et al., 2006; Salby et al., 2012; Kuttipurath et
56 al., 2013).

57 Various statistical analyses of long term total ozone column records have been performed to
58 examine the effect of external variables on total ozone using ground-based measurements (e.g.
59 Bodeker et al., 1998; Hansen and Svenøe, 2005; Wohltmann et al., 2007; Mäder et al., 2010)
60 and/or satellite measurements (e.g. Stolarski et al., 1991; Bodeker et al., 2001; Brunner et al.,
61 2006). Ground-based measurements have the advantage that they often span time periods longer
62 than those available from satellite measurements. On the other hand, satellite instruments perform
63 measurements at a higher temporal frequency (daily) and provide global coverage. Previous
64 statistical ozone studies using satellite measurements are based on zonally or regionally averaged

65 ozone data and/or ozone data averaged in equivalent latitude coordinates. The latter coordinate
66 system eliminates problems that occur when computing zonal means based on conventional
67 coordinates, like spatio-temporal variations of the polar vortex location (Pan et al., 2012).
68 However, regression studies have not yet analyzed total ozone in two geographical directions –
69 latitude and longitude – to investigate the spatial variations in regressor dependencies.

70 Ozone regression studies typically use a number of different regressors to account for non-
71 seasonal variation in stratospheric ozone. Before the year 2004, the long term trend in ozone was
72 usually modeled as a linear or piecewise linear function of time. Later, the equivalent effective
73 stratospheric chlorine and bromine (EESC) was introduced to represent the net effect of chlorine
74 and bromine on ozone (e.g. Jones et al., 2009; Mäder et al., 2010; Weber et al., 2011; Kuttippurath
75 et al., 2013). Other frequently used variables to describe natural variability in ozone are the 11-
76 year solar cycle and the quasi biennial oscillation (QBO). Some studies have indicated that the El-
77 Nino Southern oscillation (ENSO) has a significant effect on stratospheric ozone in the tropics
78 (e.g. Randel et al., 2009; Ziemke et al., 2010). In addition to these variables, the effect of
79 stratospheric aerosols caused by the volcanic eruptions of El Chicon in 1982 and Pinatubo in 1991
80 are often taken into account.

81 Several studies have linked seasonal variations in stratospheric ozone to physical variables. At
82 middle to high- latitudes, stratospheric ozone amounts are directly coupled to the Brewer Dobson
83 circulation (BDC). An important driving factor of this BDC is the vertical propagation of
84 tropospheric planetary waves, often represented by the eddy heat flux (EHF). The vertical
85 Eliassen-Palm (EP)-flux, a measure proportional to the EHF, is widely used to describe variations
86 in the BDC (e.g. Weber et al., 2011; and references therein) and to study the evolution of
87 tropospheric and stratospheric jet streams and their interaction with transient eddies (Vallis, 2007;

88 chapter 12). For ozone studies the EP-flux is mostly used to describe the polar stratospheric vortex
89 (Hood and Soukharev, 2005). This vortex forms a boundary between polar and mid-latitude
90 stratospheric air and isolates polar stratospheric ozone. This isolation has important consequences
91 for the spatial distribution and the depletion of ozone. Potential vorticity has also been reported to
92 correlate with stratospheric ozone (Allaart et al., 1993; Riishøjgaard and Källén, 1997) as is the
93 case for geopotential height (Ohring and Muenc, 1960; Braesicke et al., 2008).

94 Various methods have been applied to account for seasonality in ozone time series and the
95 seasonal variability of external forcing on ozone throughout the year, the latter from now on
96 referred to as 'seasonal ozone dependencies'. The seasonality in ozone itself and the seasonal
97 ozone dependencies are either accounted for by expanding the regression coefficients as harmonic
98 time series with periods of a year and half a year or by expanding the regression coefficients as
99 twelve indicator functions, one for each month of the year. The first approach is similar to a
100 Fourier filter on the corresponding frequencies and the latter is equivalent to performing the
101 regressions on annual data independently for each month of the year. These different methods
102 were discussed by Fioletov et al. (2008). However, no study has attempted to model ozone
103 variation in terms of physical explanatory variables only.

104 The main aim of this study is to gain a better understanding of the physical and dynamical
105 processes that affect the global distribution of ozone in longitude and latitude. We perform
106 multiple regression analysis on the extended MSR data set (van der A et al., 2010) consisting of
107 total column ozone on a $1^\circ \times 1.5^\circ$ latitude/longitude grid, spanning the time period 1979 - 2010. The
108 small grid size enables us to incorporate local and regional effects in the regression models. The
109 gridded regression results provide spatial information on ozone - regressor relations. In order to
110 achieve physically meaningful patterns we develop a physically oriented regression model (PHYS

111 model), in which both the non-seasonal and seasonal ozone variabilities are described by physical
112 explanatory variables. Also the seasonal ozone dependencies are examined and accounted for by
113 specifically constructed ‘alternative variables’. Regression results of this PHYS model are
114 compared to regression results of a statistically oriented model (STAT model), in which the
115 seasonal variation is parameterized as harmonic time series with periods of a year and half a year
116 instead of physical explanatory variables.

117 A second focus of this paper is on the quantification of stratospheric ozone recovery and the
118 role of the EESC therein. We present a global trend analysis for average ozone recovery as well as
119 specifically for the ozone hole period over Antarctica based on either EESC or piecewise linear
120 trend (PWLT) results. We also investigate the sensitivity of these results to the ‘age of air’
121 parameter in the EESC formulation and the chosen ozone recovery period as well as whether using
122 the EESC is preferred over the PWLT as measure for recovery for application in regression
123 studies.

124 This paper is organized as follows: after introducing the dependent and explanatory variables in
125 section 2.1, we briefly discuss the piecewise correlation coefficients of the explanatory variables in
126 section 2.2. Section 2.3 covers the analysis of seasonal ozone dependencies required for the
127 construction of alternative variables included in the PHYS and STAT models, which are presented
128 in section 2.4. The global spatial regression results are presented in section 3.1, while detailed
129 results for the locations Reykjavik, Bogota and the Antarctic are shown in section 3.2 to represent
130 regressions at high northern latitudes, the tropical region and high southern latitudes respectively.
131 Section 3.3 covers the trend analysis and the role of the EESC therein. Conclusions are presented
132 in section 4. A brief summary of conclusions in chapter 5 ends the paper.

133 **2. Materials and methods**

134

135 **2.1 Data overview**

136

137 **MSR ozone**

138

139 For ozone, the Multi Sensor Reanalysis (MSR) data set is used (van der A et al., 2010),
140 consisting of total column ozone data on a regular $1.5^{\circ} \times 1^{\circ}$ longitude-latitude grid. This data set is
141 based on daily assimilated measurements from the TOMS, SBUV, GOME, SCIAMACHY, OMI
142 and GOME-2 satellite instruments spanning the time period 1978-2008. Independent ground-based
143 measurements from the World Ozone and Ultraviolet Data Center (WOUDC) were used for
144 correction of biases between the different satellite measurements. Dependencies on solar zenith
145 angle, viewing angle, time and stratospheric temperature were taken into account in the bias
146 correction scheme. The MSR data set consists of monthly ozone averages and the standard
147 deviations corresponding to these averaged values as a measure for the spread of ozone values
148 within corresponding months. The MSR is extended with two years (2009 and 2010) of monthly
149 averaged assimilated ozone measurements from SCIAMACHY on the same grid (Eskes et al.,
150 2005). The SCIAMACHY measurements are corrected for biases in the same way as for satellite
151 measurements in the MSR. The final data set contains 32 years of gridded total column ozone data.

152

153 **EESC / Long term variability**

154

155 The long term variability in ozone is highly correlated to the abundance of the halogens listed in
156 the quadrennial scientific assessment of ozone depletion (WMO 2010, and references therein).
157 Mäder et al. (2010) suggested that the long term ozone variability due to halogen species is best
158 described by the equivalent effective stratospheric chlorine (EESC) rather than a piecewise linear
159 function. To represent the long term variability as an explanatory variable, we therefore use the
160 EESC (Newman et al., 2007). The calculation of this variable is based on the amount of bromine
161 and chlorine atoms in various source gasses, the mixing ratio of these gasses in the stratosphere
162 and the efficiency of these gasses in terms of halogen release. In the EESC calculation used for the
163 global gridded regressions, the age of air and the corresponding spectrum width parameters are set
164 to 5.5 years and 2.75 years, respectively. This choice is based on our specific interest in polar
165 stratospheric ozone depletion where the air age is assumed around 5.5 years. All other parameters
166 are set at default: the WMO/UNEP 2010 scenario, the WMO 2010 release rates, inorganic
167 fractional release rates and a bromine scaling factor of 60. However, the use of one fixed age of air
168 for all stratospheric ozone is a gross oversimplification. Stiller et al. (2012; their figure 7) show
169 that the age of air is strongly height and latitude dependent. The age of air can vary from a few
170 years in the tropics and the lowermost stratosphere at high latitudes to more than 10 years in the
171 upper stratosphere. Hence, to test the sensitivity of our analysis for choices in the age of air we
172 compare regression results with the EESC using air ages of 3, 4 and 5.5 years (1.5, 2 and 2.75
173 years for corresponding spectrum widths, respectively) and PWLT analysis for straightforward
174 recovery rate quantification. Note that results of this study will be analyzed for identifying the
175 ‘best’ regression model and trend estimator.

176

177 **Solar cycle**

178

179 Absorption of incoming UV radiation is a crucial mechanism for stratospheric ozone formation
180 and affects ozone amounts. The eleven-year solar cycle dominates the incoming UV radiation
181 (Lean et al., 1989) and has been identified in many ozone records (e.g. Shindell et al., 1999). A
182 commonly used proxy to characterize the UV radiation in ozone regression studies is the 10.7cm
183 Solar Flux data (NOAA), provided as a service by the National Research Council of Canada. The
184 monthly data set is generated by daily measurements of the solar flux density at 2800 MHz, taken
185 by radio telescopes at Ottawa (until May 31, 1991) and Penticton (from July 1st 1991).
186 Measurements were taken at local noon time, and corrected for several measurement factors to
187 reach an accuracy of a few percent. We denote this explanatory variable by ‘SOLAR’. See
188 <http://www.ngdc.noaa.gov/stp/solar/flux.html> for the data and more information.

189

190 **Stratospheric aerosols**

191

192 To account for the effect of stratospheric aerosols (AERO) we use time series of stratospheric
193 aerosols as described by Sato et al. (1993; for an update, see Bourassa et al., 2012). These data are
194 based on measurements from the satellite instruments SAM II and SAGE as well as observations
195 from several ground stations. This data set consists of twenty-four monthly time series
196 corresponding to 7.5 degree latitudinal bands of averaged amount of stratospheric aerosols. Data is
197 taken at a height of 20-25 km. Aerosols taken at other stratospheric height levels are positively
198 correlated and are, therefore, not included. For instance, the correlation coefficient between
199 aerosols at 20-25 km and those at 15-20 km is 0.62. The El Chicon (1982) and Pinatubo (1991)
200 volcanic eruptions dominate the stratospheric aerosol time series.

201

202 **QBO**

203

204 The effect of the Quasi-biennial Oscillation (QBO) in easterly and westerly stratospheric winds
205 at the tropics on stratospheric ozone is a well-established effect based on both observations and
206 stratospheric modeling and is known to affect stratospheric ozone outside the tropics as well
207 (McCormack et al., 2007; Witte et al., 2008; WMO 2010, chapter 2, and references therein). The
208 QBO is represented by time series of monthly averaged wind speed measurements done by the
209 ground station in Singapore (Baldwin et al., 2001). Time series of wind speeds measured at 30 and
210 10 hPa are included to account for differences in the phase and shape of the QBO signal at these
211 heights. We considered adding a proxy to represent the QBO at 50 hPa but rejected this because of
212 the high anti-correlation with the QBO at 10 hPa (correlation value of -0.69).

213

214 **El Nino/Southern Oscillation (ENSO)**

215

216 Various studies have shown that the ENSO signal affects the dynamics of the lower
217 stratosphere, including the amount of ozone (e.g. Randel et al., 2009; Ziemke et al., 2010). The
218 Multivariate ENSO Index (MEI) (Wolter and Timlin, 1998) is used to represent the effect of the
219 ENSO. Sea-level pressure, zonal and meridional surface winds, sea surface temperature, surface
220 air temperature and cloud fraction are used to calculate this index.

221

222 **Eliassen Palm flux**

223

224 At mid to high latitudes the dynamical features in the stratosphere, such as the polar vortex, are
 225 highly affected by vertical propagation of tropospheric planetary waves. The vertical Eliassen-
 226 Palm flux (EP) (Kanamitsu et al., 2002) is used as a measure of the force of this vertical
 227 propagation and the stability of these polar vortices. For the Northern and Southern Hemisphere
 228 we characterize these variables by averaging the vertical component of the EP-flux at 100 hPa over
 229 45°N–75°N and 45°S–75°S separately and denote these variables as EP-N and EP-S, respectively.
 230 A strong vortex isolates the polar stratospheric air and enables the formation of an ozone hole.
 231 This isolation affects the amount of ozone cumulatively in time, with larger cumulative effects in
 232 the buildup phase as compared to the rest of the year. Therefore we adjust the time series as in
 233 Brunner et al. (2006):

$$234 \quad x_{EP}(t) = x_{EP}(t-1) \cdot e^{\frac{1}{\tau}} + \tilde{x}_{EP}(t) \quad (1)$$

235 where X_{EP} is the final EP-flux time series, \tilde{X}_{EP} the original EP-flux time series from the NCEP
 236 Reanalysis and τ set to 12 months from October to March in the Northern Hemisphere (and shifted
 237 six months for the Southern Hemisphere) and set to 3 months for the rest of the year. Note that the
 238 EP flux is also indicative for the transport of ozone rich air from the tropics towards mid-latitudes,
 239 which should be considered in the interpretations of EP flux regression results.

240

241 **Geopotential Height and Potential Vorticity**

242

243 The ECMWF reanalysis provides the geopotential height (GEO) at 500 hPa and the potential
 244 vorticity (PV) at 150 hPa as gridded monthly averaged fields. These variables are used as
 245 measures for the tropopause height and the mixing ratio of air between the troposphere and the

246 stratosphere, respectively. These variables are taken at corresponding pressure levels to account
247 for vertical propagation of tropospheric dynamics.

248

249 **Length of day**

250

251 Finally, the monthly average day length (DAY) is calculated for each latitude to describe the
252 amount of exposure to solar radiation. Therefore, this variable accounts for the direct local effect
253 of radiative variations on ozone.

254

255 Table 1 lists all variables and their sources. All time series of these explanatory variables are
256 normalized by subtracting their mean values and dividing by their standard deviation. The
257 normalized variables are shown in Figure 1. We separate the explanatory variables in two groups;
258 group A includes EESC, SOLAR, QBO, AERO and ENSO, which do not contain a seasonal
259 component and group B includes EP, GEO, PV and DAY, which are dominated by a seasonal
260 component.

261

262 **2.2 Correlations between explanatory variables**

263

264 High correlation values between regression variables may cause problems for the estimation of
265 regression coefficients as it hampers attributing variations in ozone to one particular explanatory
266 variable in both performing the regression and interpretation of results (see also Mäder et al.,
267 2010). The correlations between the variables of group B are considered separately because GEO,
268 PV and DAY are gridded data sets. Table 2 shows the (piece-wise) correlation values of the

269 variables of group A and EP. Due to the large correlation value (0.52) between both EP variables,
270 we use EP-N and EP-S only in the Northern and Southern Hemisphere, respectively.

271 The correlations between the variables of group B are shown in Figure 2. Most of these
272 variables are highly correlated at middle to high-latitudes. Regression runs show considerable
273 sensitivity to these variables south of 55°S. Among the group B variables we therefore choose to
274 use only PV and EP south of 55°S. The correlations between EP and DAY are nearly constant in
275 both hemispheres, attaining correlation values of approximately -0.69 in the Northern Hemisphere
276 and 0.17 in the Southern Hemisphere. Despite these high correlations at the Northern Hemisphere,
277 preliminary regressions with both of these variables included and either one of them included
278 separately showed reasonable robustness of the obtained results up to approximately 50°N,
279 whereas at high latitudes the high correlations complicate interpretation of the regression results.
280 For this reason we choose to include both EP and DAY for regressions performed at the Northern
281 Hemisphere.

282

283 **2.3 Analysis of seasonal ozone dependencies**

284

285 Linear regressions are performed on normalized data averaged along geographical latitudes,
286 with regression estimates expanded as 12 indicator functions, one for each month, to examine the
287 seasonality in the regression coefficients. A linear regression model is used of the form

$$288 \quad Y = \sum_{i=1}^{12} I_i \cdot a_i + \sum_{j=1}^m \sum_{i=1}^{12} I_i \cdot \beta_{i,j} \cdot X_j + \varepsilon \quad (2)$$

289 where Y is a vector of monthly ozone values, I_i the indicator function for month i of the year, a_i the
290 intercept coefficient of month i of the year, m the amount of explanatory variables, X_j the

291 explanatory variable j , β_{ij} the regression estimate for month i of variable X_j and ε the noise vector.
292 The explanatory variables of group B are not included in these regressions. Since these seasonal
293 variables are meant to parameterize seasonal variation in ozone, additionally incorporating
294 seasonal ozone dependencies for variables of group B would create problems with respect to the
295 few degrees of freedom in seasonal ozone variation using monthly data.

296 We use the least squares estimation for the regression coefficients and perform an iterative
297 backwards variable selection method similar to Mäder et al. (2007) to increase the degrees of
298 freedom in the regressions. For each iteration the P-values of two-sided T-tests corresponding to
299 the regression coefficients are calculated. The variable with the largest P-value which also exceeds
300 a chosen significance level α is excluded in the following estimation step. This procedure is
301 iterated until all P-values are below α . In these regressions we set α at 0.1, corresponding to a
302 significance value of 90%. This rather loose significance value is chosen because at this point we
303 are not interested in the significance of the regression estimates, but only in the seasonal patterns
304 obtained in these regression estimates.

305 Figure 3 shows the regression coefficient estimates for the explanatory variables of group A.
306 These estimates are used to determine the seasonal ozone dependencies, and construct
307 corresponding ‘alternative variables’ to account for this effect. Except for the EESC variable, we
308 characterize these seasonal ozone dependencies by specific harmonic functions. The seasonal
309 ozone dependency of the EESC is constructed using the averaged corresponding regression
310 coefficients poleward of 65°S.

311 For the QBO at 30 hPa a strong seasonal variation in the estimates at mid-latitudes is present.
312 This seasonality is modeled by a cosine starting its period in March. This harmonic function
313 follows the observed seasonality at 30°S, and has an opposite relation to the regression estimates at

314 30°N (Figure 3). For the QBO at 10 hPa the seasonality in the regression estimates is described as
315 a cosine starting its annual cycle in February. This function again aligns with the variation in
316 obtained regression estimates around 30°S and has an opposite relation to those at around 30°N.

317 Regression estimates corresponding to the ENSO variable show different values in the months
318 from July to September in comparison to the rest of the year. This effect is modeled using a cosine
319 with its peak in August.

320 The results show no convincing seasonal pattern in the estimates corresponding to the variables
321 SOLAR and AERO. Therefore, no alternative variables are included to account for seasonal ozone
322 dependencies of SOLAR and AERO.

323 The seasonal ozone dependency of EESC in Polar Regions does not have a harmonic shape due
324 to the ozone hole occurring essentially from September to November. To construct the alternative
325 variable to parameterize EESC's seasonal ozone dependency, we average the regression
326 coefficients from the above regression in latitudes poleward of 65°S for each month obtaining a
327 32-year seasonal function $S(t)$. Assuming this seasonality in ozone dependency had marginal
328 effects before 1979, we multiply the obtained seasonal function $S(t)$ with the increase of EESC at
329 month t with respect to its 1979 value. The above assumption is justified because the seasonal
330 effect of ozone depleting substances on ozone was marginal before 1980 (e.g. Li et al., 2009).
331 Because we don't find results in Figure 3 corresponding to the Arctic ozone hole, we do not define
332 an alternative variable for the Arctic polar region. Year-to-year variability in Arctic ozone
333 depletion is much larger due to a less stable Arctic stratospheric vortex (Douglass et al., 2011)
334 such that a well-defined Arctic ozone hole is rare.

335 Based on the observations made above, the alternative variables QBO30_2, QBO10_2,
336 ENSO_2 and EESC_2 to account for seasonally varying dependencies are defined as follows:

$$\begin{aligned}
337 \quad & \text{QBO30}_2(t) = \cos(2\pi(t - 2)/12) \cdot \text{QBO30}(t) \\
& \text{QBO10}_2(t) = \cos(2\pi(t - 1)/12) \cdot \text{QBO10}(t) \\
& \text{ENSO}_2(t) = \cos(2\pi(t - 8)/12) \cdot \text{ENSO}(t) \\
& \text{EESC}_2(t) = (S(t) - \text{mean}(S)) \cdot (\text{EESC}(t) - \text{EESC}(0)),
\end{aligned} \tag{3}$$

338 where t is the time in months from January 1979 and $S(t)$ is described above. These alternative
339 variables are normalized after construction, as was done for other explanatory variables. Note that
340 these alternative variables are not necessarily dominated by the multiplied seasonal function. This
341 is only the case for EESC_2 , due to the extremely low short term variations in EESC. EESC_2
342 shows a very specific trend in this seasonality which is very different from the highly seasonal
343 variables in group B. Therefore, the alternative variables do not interfere much with the
344 parameterization of seasonal ozone variability in the regression models that are defined in the next
345 section.

346

347 **2.4 Regression methods**

348

349 As mentioned before, we construct a physically oriented model (PHYS) where the non-seasonal
350 ozone variations are accounted for by the physical explanatory variables of group A, their seasonal
351 ozone dependencies are described by specific alternative variables and the seasonal ozone
352 variation is described by the variables of group B. The multi linear regressions are performed
353 using the linear model

354

$$355 \quad Y = \beta \cdot X + \varepsilon \tag{4}$$

356

357 where Y is the vector of monthly averaged ozone values, X the matrix with the explanatory
358 variables as columns including an intercept as a column of ones, β the vector of regression

359 coefficients corresponding to the columns of \mathbf{X} and $\boldsymbol{\varepsilon}$ the noise vector with entries assumed to be
 360 uncorrelated and standard normal distributed. This assumption is a simplification since
 361 autocorrelation does affect the uncertainty in regression estimates. Considering that we are
 362 interested only in the geographical patterns that arise in the regression results and not the specific
 363 values of statistical errors this simplification is justified. In case of the trend analysis, where
 364 statistical significance has an important role, we calculate the error of the PWLT (piecewise linear
 365 trend variable, as defined below) and the EESC regression coefficient as (Press et al., 1989)

$$366 \quad \sigma^2 = (\mathbf{X}^T \mathbf{X})^{-1} \cdot \frac{\sum_t ((Y - \boldsymbol{\beta} \cdot \mathbf{X})(t))^2}{n-m} \cdot \frac{1+\phi}{1-\phi},$$

367 where σ denotes the vector of regression errors corresponding to the regression estimates $\boldsymbol{\beta}$, n is
 368 the length of the time series in months, m is the amount of fitted parameters and ϕ the estimated
 369 lag 1 autocorrelation of the residuals.

370 The regression coefficients are estimated using the weighted least squares method, with weights
 371 reciprocal to the variance of the monthly averaged ozone values. The backwards selection
 372 algorithm as described in section 2.3 selects the explanatory variables based on significance value
 373 set to 0.01 corresponding to a significance value of 99%.

374 For comparison, a rerun of these regressions is performed with a statistically oriented model
 375 (STAT). This model differs from the above model only in the parameterization for the seasonal
 376 ozone variations. The PHYS model uses physical variables PV, GEO, EP and DAY to describe
 377 ozone variation whereas the STAT model uses harmonic time series with periods of a year and
 378 half a year for this parameterization. This method, similar to a Fourier filter on seasonal and sub-
 379 seasonal frequencies, is widely applied in former ozone regression studies (e.g. Fioletov et al.,

380 2008). Table 3 shows an overview of the incorporated explanatory variables for both the PHYS
381 and the STAT model.

382 Finally, several regression runs are performed with specific focus on trend analysis and the role
383 of EESC on ozone recovery. An important parameter in the calculation of EESC is the age of air in
384 which the alternative halogens are contained. Differences in this parameter ultimately lead to
385 differences in the rate of ozone recovery due to different shape of the resulting EESC time series.
386 We perform trend analyses using results of the PHYS model with the EESC variable at air ages 3,
387 4 or 5.5 years or substituted by a piecewise linear function with its second linear component
388 spanning 1997-2010, 1999-2010 or 2001-2010. The piecewise linear trend (PWLT)
389 characterization for long term ozone variation has the advantage that the slope in ozone recovery
390 and ozone depletion periods can be estimated separately, whereas these slopes are proportionally
391 fixed in the EESC curves. On the other hand the EESC parameterization yields a smooth transition
392 from the fast early increase to the more recent gradual decrease rather than the ad-hoc turn around
393 point in the PWLT characterization.

394

395 **3. Results**

396

397 **3.1 Multi-linear regression results**

398

399 The multi-linear regression results for non-seasonal variables are shown in Figure 4. The EESC,
400 characterizing the long term ozone variation, has a negative effect on ozone outside the tropics
401 with the largest effect in the Southern Hemisphere. No significant results for EESC were found in
402 the tropical region. The negative EESC related ozone effects at mid- to high latitudes are in

403 agreement with current understanding of EESC driven ozone depletion. The ozone hole over
404 Antarctica is parameterized by the alternative variable EESC_2 for which by construction the
405 corresponding regression estimates are positive. Characterizing the EESC driven occurrence of an
406 ozone hole over Antarctica, the EESC_2 regression coefficients are large in this region. These
407 estimates attain values indicative of ozone fluctuations up to 90 DU in magnitude at the Antarctic
408 in the year 2001, when the EESC attains its peak. Further quantitative analysis regarding ozone
409 recovery rate and the role of EESC therein is performed in section 3.3.

410 The 11-year solar cycle positively affects ozone at low and mid-latitudes, mainly in the
411 Southern Hemisphere. At the equator the regression coefficients are barely significant. The
412 positive sign in these regression estimates is consistent with the role of UV radiation in ozone
413 formation processes.

414 Stratospheric volcanic aerosols affect stratospheric ozone negatively due to catalytic ozone
415 depletion on the surface of aerosol particles (Solomon et al., 1996). This results in negative
416 regression estimates corresponding to this variable, mainly seen North of 45°N.

417 The dependence of ozone on QBO shows clear spatial patterns. Positive regression estimates
418 corresponding to the QBO index for the two pressure levels indicate a positive effect on ozone
419 along the equator. Moving towards higher latitudes the regression estimates switch to negative
420 values at approximately 10°N and 10°S. For the QBO at 30 hPa the estimates remain negative up
421 to 60°S for the Southern Hemisphere and up to the Arctic region for the Northern Hemisphere,
422 whereas the regression estimates corresponding to the QBO at 10 hPa the regression estimates
423 switch back to positive values around 50°N and 50°S.

424 The ENSO regression estimates show negative ozone effects of El Nino between 25°S and
425 25°N, especially over the Pacific. The corresponding alternative variable ENSO_2 does not
426 contribute significantly in this regression model.

427 Figure 5 shows the regression estimates corresponding to the seasonal variables of group B.
428 The variable DAY - accounting for variations in radiative forcing - has the largest regression
429 coefficients. The EP regression estimates show the different effect of EP on ozone poleward and
430 equatorward of the polar vortex in both hemispheres. The average location of the Antarctic vortex
431 is located along a band at approximately 60°S where the EP regression coefficient changes sign.

432 The estimates corresponding to DAY are almost entirely positive throughout both hemispheres,
433 without much spatial variability. Contrary to the DAY results, the EP results in the Northern
434 Hemisphere show a change in sign from the tropics (negative) to higher latitudes (positive).

435 Significant regression results for PV are mainly found over the Arctic and Antarctic. For the
436 Antarctic these effects also interact with the effects of DAY and EP variables on ozone where
437 these strongly correlate to PV (see Figure 2). The sign difference in estimates between both
438 hemispheres is due to the sign change of potential vorticity at the equator. As a result, the effect of
439 vorticity at the 150 hPa pressure level on ozone appears to be rather similar for both hemispheres.
440 Ozone variations are negatively related to geopotential height (GEO) poleward of 30°N and
441 around 50°S.

442 One possible interpretation of the regression results for DAY and EP is that DAY represents the
443 seasonal changes in photochemistry, whereas EP represents the seasonally varying transport
444 processes from source regions (tropics) to sink regions (higher latitudes). As reported in Miyazaki
445 et al. (2005), stratospheric transport from the tropics to the Northern Hemisphere is stronger
446 compared to the Southern Hemisphere. They also note that in the Southern Hemisphere the mean

447 transport does not extend beyond the polar vortex, whereas the eddy transport does, contrary to the
448 Northern Hemisphere, where both mean and eddy transport contribute to transport to high
449 latitudes. This suggests that the EP regression represents ozone transport. However, due to
450 correlations of DAY with especially EP care has to be taken when interpreting these results and
451 the EP regression estimates at high northern latitudes. South to 55°S the effects of DAY and PV
452 interact because these variables are strongly correlated (see Figure 2).

453

454 **3.2 Comparison with STAT model results**

455

456 The regression results discussed in section 3.1 are compared with those from the STAT model,
457 in which seasonal ozone variations are parameterized by harmonic time series with periods of a
458 year and half a year, similar to a Fourier filter on the most prevalent frequencies. We compare
459 results corresponding to the non-seasonal variables of group A, and investigate whether seasonal
460 variation is properly parameterized in the physical model by comparing the explanatory powers of
461 both models in terms of R^2 , defined as one minus the fraction of residuals sum of squares divided
462 by the sum of squares in the dependent variable. Regressions of both methods performed at
463 Reykjavik, Iceland (64°N, 23°W), Bogota, Colombia (5°N, 74°W) and the Antarctic (80°S, 0°E)
464 are shown in detail to gain a thorough impression of both methods at these selected sites. These
465 three sites are considered typical for the Northern Hemisphere mid-latitudes with large seasonal
466 variation, tropics with a large influence of QBO and ENSO and the Antarctic vortex area.

467 First we compare results of the non-seasonal variables obtained by the STAT model (Figure 6)
468 with those obtained by the PHYS model (Figure 4). Although nearly all of these coefficient maps
469 show similar spatial patterns, differences are found. Small differences are in the model

470 contribution of EESC and AERO, as the corresponding regression coefficients for these variables
471 EESC at high northern latitudes are higher in the PHYS model than in the STAT model. More
472 interestingly, the ozone hole characterization by EESC_2 is less obvious in the STAT model
473 results in comparison to the PHYS model results, the reason for this difference will be clarified
474 describing the detailed results of Antarctica. The QBO and ENSO variables, both the original and
475 alternative variables, show latitudinal wider and stronger impact on ozone in the STAT model
476 results than for the PHYS model results (Figure 6 and Figure 4, respectively). The influence of the
477 QBO variables extends up to the Arctic region in the STAT model results, as compared to nearly
478 40°N for the PHYS model. Regarding the ENSO results, bands of positive regression estimates for
479 the STAT model are present at approximately 40°N and 40°S, possibly indicating an El Nino
480 circulation pattern at mid-latitudes. Furthermore ENSO_2 does indicate some seasonal effect in
481 ENSO - ozone dependency. The corresponding spatial pattern is in agreement with results shown
482 in Figure 3.

483 Both model's performance in term of R^2 are compared to investigate how well the PHYS model
484 describes seasonal variations in ozone. Assuming the seasonal variation in ozone is completely
485 filtered out in the STAT model using orthogonal harmonic time series, similar R^2 values for the
486 PHYS regressions with respect to the STAT regressions are indicative of a fully physically
487 characterized seasonal ozone component in the PHYS model. The R^2 values, as presented in
488 Figure 10, show similar spatial patterns for both models, except for the region north of 70°N,
489 where the STAT model achieves higher explained variance. The average R^2 value obtained by the
490 PHYS model, 0.72, is nearly at the same level as 0.79 that is (on average) achieved by the STAT
491 model. Excluding latitudes north of 70°N in the averaging, these values are 0.73 and 0.78,
492 respectively.

493 Detailed results from the PHYS and STAT regressions at Reykjavik, Bogota, and the Antarctic
494 are shown in Figures 7, 8 and 9. Corresponding regression coefficients are presented in tables 4, 5
495 and 6, respectively, together with their standard errors. The “Fourier” term in these figures is
496 defined as the sum of the harmonic components that describe seasonal ozone variation in the
497 STAT model. For Reykjavik, QBO variables were found significant in the STAT model (right plot
498 in Figure 7) but were not found significant in the PHYS model (left plot in Figure 7). Furthermore,
499 the seasonal component in the PHYS model is described by a combination of mainly the PV, DAY
500 and EP variables. At Bogota, only the ENSO_2 alternative variable has been excluded in the
501 PHYS regression compared to the STAT regression (Figure 8). The seasonal component is
502 parameterized by only the EP and a small contribution of GEO. For the Antarctic (Figure 9) a
503 large difference exists in the way both methods account for the ozone hole. In the STAT regression
504 this phenomenon is mainly described as a stationary seasonal variation using harmonic time series,
505 with a smaller role for the constructed EESC_2, whereas the PHYS regression attributes two times
506 more variation to EESC_2. The PV and EP variables complete the seasonal parameterization in the
507 PHYS model.

508

509

510 **3.3 Ozone recovery**

511

512 An important topic of the current debate in ozone research is the detection of ozone recovery
513 attributable to the decrease in EESC, for which a number of recent studies have relied on
514 regression methods (Salby et al., 2011, 2012; Kuttippurath et al., 2013). In addition to the average
515 ozone recovery, particular interest exists in the recovery of ozone over Antarctica during the ozone

516 hole period (September - November). Both the average and the ozone hole recovery rates are
517 quantified using EESC regression estimates from the PHYS model and by PWLT analysis. Results
518 are significant at the 99% confidence interval.

519

520 **3.3.1 Average ozone recovery**

521

522 The first quantification for the average ozone recovery rate is based on the PHYS regression
523 results. The average ozone recovery rate is estimated by multiplication of the EESC regression
524 coefficient with the average rate of change in EESC since it obtained its peak value (1997, 1999 or
525 2001 for 3, 4 or 5.5 year air age respectively).

526 As a second trend quantification method PHYS regression runs are performed in which a
527 piecewise linear function substitutes the EESC as parameterization for long term ozone variation.
528 The piecewise linear function consists of a linear component from 1979 to 2010 and a component
529 linear in either 1997-2010, 1999-2010 or 2001-2010 time periods and zero prior to this period. The
530 ozone recovery rate in the latter time period is quantified by the sum of both linear components
531 multiplied by their regression coefficients.

532 Results of both methods are shown in Figure 11. We notice that EESC related ozone recovery
533 rate estimates (the upper plots in Figure 11) are highly dependent on the age of air parameter used
534 for the EESC variable (Table 7). Assuming an air age of 3 years, the average ozone recovery rate
535 is 0.7 DU/year for the Southern Hemisphere (excluding the Antarctic ozone hole area) and 0.6
536 DU/year for the Northern Hemisphere. For air ages of 4 and 5.5 years, these values are 0.5 and 0.3
537 DU/year, respectively, for the Southern Hemisphere and 0.4 and 0.2 DU/year, respectively, for the
538 Northern Hemisphere. The 3 year air age EESC related ozone recovery rates are found significant

539 towards the tropical region, whereas the 5.5 year air age EESC related recovery rates are found
540 significant only poleward of 10°S and 30°N.

541 The PWLT analysis provides higher ozone recovery rate estimates than the EESC. Linear
542 recovery rate estimates spanning 1997-2010, 1999-2010 and 2001-2010 periods are approximately
543 0.7, 1.0 and 1.4 DU/year, respectively, for the Southern Hemisphere and 1.0, 1.3 and 1.7 DU/year,
544 respectively, for the Northern Hemisphere.

545 Note that in particular the Southern Hemisphere recovery rates for the PWLT analysis are not or
546 barely statistically significant.

547

548 **3.3.2 Ozone hole recovery**

549

550 A particular interest is in the recovery of Antarctic ozone in September - November
551 months, corresponding to the ozone hole period. Two methods are used to quantify the ozone
552 recovery in this specific time period.

553 First, estimates for ozone recovery rate for the ozone hole are generated by multiplication of the
554 EESC_2 regression coefficients with the average increase in EESC_2's yearly minima per year
555 after its largest oscillation. These recovery rates are summed with the average EESC related
556 recovery rates, as calculated in the previous section (upper plots in Figure 11). We obtain results
557 corresponding to 3, 4 and 5.5 year air age EESC variables. Second, a PWLT analysis is performed
558 on yearly ozone time series of ozone averaged over September - November months. This analysis
559 is performed by again using 1997-2010, 1999-2010 or 2001-2010 as ozone recovery periods.

560 Ozone recovery rates are shown in Figure 12 for both methods. Again we note large differences
561 in ozone recovery rate estimates for different air age parameters and different periods for recovery

562 rates in PWLT analysis. EESC related ozone hole recovery rate estimates vary between around
563 1.8, 1.4 and 0.9 DU/year for EESC variable with 3, 4 and 5.5 year air ages, respectively. For
564 PWLT results the estimates at the Antarctic vary between around 1.3, 2.3 and 3.1 DU/year for
565 ozone recovery periods 1997-2010, 1999-2010 and 2001-2010, respectively. The PWLT results in
566 September - November show a larger recovery rate over Antarctica than anywhere else, related to
567 the larger amount of ozone depletion within the Antarctic ozone hole in the September to
568 November period. The PWLT analysis yield higher ozone recovery rates than those obtained by
569 using the EESC curve. However, although each linear segment has been included at the 99%
570 significance level, none of the PWLT recovery rates are statistically significant. The reason for this
571 insignificance is that the regression coefficients of both linear segments have been summed to
572 achieve the total recovery rate estimates. Processing the corresponding standard errors increases
573 the final standard error.

574

575 **4 Discussion**

576

577 The spatially applied regressions provide spatial parameterization of ozone in terms of
578 physical explanatory variables. The results show larger effects of EESC on ozone in the Southern
579 Hemisphere than at the Northern Hemisphere and increase towards higher latitudes. This results
580 from ozone being produced at the tropics and transported to higher latitudes so that ozone at higher
581 latitudes has been affected by ozone depleting substances for a longer time period. A similar
582 hemispheric asymmetry, with larger ozone influences at the Southern Hemisphere, is found in the
583 effect induced by the solar cycle, having positive regression coefficients at low- and mid- latitudes
584 for both hemispheres and barely significant regression coefficients at the equator itself. This

585 spatially persistent but weak solar signal is consistent with results of Soukharev and Hood (2006)
586 on the solar cycle variation in ozone and Wohltmann et al. (2007). This solar signal extends up to
587 more than 70°S between -50° and 100° in longitudes according to our results.

588 The negative effect of stratospheric aerosols particularly at high northern latitudes supports
589 earlier findings of for example Solomon et al. (1996). Interestingly, the impact of volcanic aerosols
590 on stratospheric ozone has also been discussed extensively for the Southern Hemisphere and
591 Antarctic based on observations (Deshler et al., 1992; Hofmann and Oltmans, 1993), model
592 simulations (Knight et al., 1998; Rozanov et al., 2002) and regression analysis (Brunner et al.,
593 2006; Wohltmann et al., 2007; Kuttippurath et al., 2013). Yet, in our analysis we find little
594 evidence of Antarctic ozone being affected by volcanic aerosols. One possible explanation could
595 be that to some extent Antarctic volcanic aerosol effects are compensated for by the EP flux and/or
596 Antarctic Oscillation effects (see Figure 5 of Kuttippurath et al. (2013) and Figure 4 of Brunner et
597 al. (2006)). Note that the Pinatubo eruption had a smaller impact on the Southern Hemisphere
598 (Robock et al., 2007). In addition, modeling results by Knight et al. (1998) suggest that the largest
599 Southern Hemisphere effects of the Pinatubo eruption occur outside of the Antarctic vortex, a
600 finding that is supported by Hofmann et al. (1997) and Solomon et al. (2005; their Figures 3 and
601 13) who report only major effects of Pinatubo on ozone in the upper troposphere and lowermost
602 stratosphere. Furthermore, results from a modeling study by Rozanov et al. (2002) only find
603 statistically insignificant decreases in Antarctic ozone due to volcanic aerosols, suggesting other
604 large influences on Antarctic ozone. Finally, the majority of publications identifying an effect of
605 Pinatubo on Antarctic ozone were published in the 1990s, a period during which the role of extra-
606 tropical dynamics like the EP-flux on Antarctic ozone were poorly known (this started to be
607 discussed after the year 2000).

608 We found broad spatial patterns concerning the QBO - ozone relation, which is positive at
609 the equator and changes to negative at around 10°N and 10°S for QBO taken at both 10 and 30
610 hPa. These results are in agreement with Brunner et al. (2006) and Yang and Tung (1995) on the
611 phase propagation of the QBO signal in ozone data. The negative effects on ozone induced by
612 ENSO events, detected between 30°N and 30°S particularly over the Pacific, are consistent with
613 findings by Randel et al. (2009). The STAT model additionally identifies positive ENSO related
614 effects in small bands at 40°N and 40°S. This result may indicate an ENSO effect on stratospheric
615 ozone transport from the equator - and the Pacific in particular - towards higher latitudes.

616 Interestingly, as the STAT model attributes more ozone variation to QBO and ENSO
617 variables at higher northern latitudes as compared to PHYS model results, the PHYS results show
618 a more persistent pattern of EESC and AERO ozone effects at high northern latitudes. The
619 different characterization of seasonal variation in ozone in these models causes these small
620 differences. Another difference is found in the EESC_2 results over Antarctica where a large part
621 of ozone variations that could be interpreted as EESC driven according to the PHYS model
622 (Figure 9) is accounted for by harmonic variables in the STAT model.

623 The important gain of the PHYS model with respect to the STAT model is the physical
624 parameterization of seasonal ozone variation in terms of DAY, EP, PV and GEO. Except for a
625 small band at the equator, regressions estimates show a positive effect on ozone attributed to the
626 explanatory variable DAY, which represents the variation in local exposure to solar radiation. In
627 the interpretations of these results, we must account for the high correlation values between EP
628 and DAY at the Northern Hemisphere. Up to around 50°N, the positive effect of DAY on ozone is
629 mostly due to in situ ozone production driven by exposure to solar radiation. Towards higher
630 latitudes the DAY regression coefficients are increasingly affected by correlation features with the

631 EP variable complicating direct physical interpretations due to overestimation of regression
632 coefficients. The increasingly positive EP results towards high latitudes are a result of ozone
633 transport driven by the Brewer Dobson circulation. At the Southern Hemisphere the EP results
634 show different effects on ozone poleward and equatorward of the southern polar vortex, related to
635 the separation of stratospheric air within the polar vortex. The much larger EP regression
636 coefficients north of 40°N compared to the Southern Hemisphere shows that eddy heat flux affects
637 Arctic stratospheric ozone more than Antarctic stratospheric ozone. This is due to a much stronger
638 effect of wave dynamics leading to less stability of the polar vortex in the Northern Hemisphere
639 compared to the Southern Hemisphere (Randel et al., 2002).

640 Synoptic scale weather variability, represented by PV at 150 hPa, has a positive effect on
641 ozone, especially at high latitudes. South of 55°S the results of PV partly account for ozone effects
642 of DAY, GEO and EP variables, which are correlated with PV. Finally ozone is affected
643 negatively by high values of geopotential height at 500 hPa in southern mid-latitudes and northern
644 mid to high-latitudes. The importance of synoptic scale meteorological variability in understanding
645 extra-tropical total ozone column variability has long been recognized (e.g. Harris et al., 2008;
646 Kieseewetter et al., 2010; Rieder et al., 2010).

647 The explanatory power of the PHYS model nears the explanatory power of the STAT
648 model in regressions performed south of 70°N (R^2 values of 0.73 to 0.78, respectively). Assuming
649 the seasonal ozone component is completely accounted for in the STAT model using a Fourier
650 filter we conclude that the PHYS model also accounts for nearly all seasonal variation in ozone,
651 since the models differ only in the parameterization for seasonal ozone variation. The higher
652 performance of the STAT model as compared to the PHYS model north of 70°N is caused by
653 extreme domination of stable seasonal variations in the ozone time series, which are better

654 parameterized by the orthogonal harmonics in the STAT model. Regions where both regression
655 models yield lower explanatory power are bands at around 55°S, 10°S and a smaller band over
656 northern Africa stretching towards the central part of Asia. The reduced explanatory power at 55°S
657 is related to the vortex edge itself. Regression studies focusing on the Antarctic ozone hole
658 typically use either a dynamical definition like the equivalent latitude to define the vortex area, or
659 stay sufficiently far away from the vortex edge (south of 70°S; e.g. Kuttipurath et al. (2013)).
660 Hassler et al. (2011) shows that the shape of the Antarctic vortex has changed somewhat during
661 the last 30 years which has consequences for analyzing Antarctic ozone. However, given that this
662 study focuses on the global patterns of ozone variability, use of a spatially variable definition of
663 the vortex edge is not possible. The other bands at 10°S and from northern Africa to Central Asia
664 are regions of low ozone variability. These ozone time series are dominated by white noise and
665 are, therefore, unexplained by the regression models.

666 The EESC trend analysis shows significant ozone recovery in the Southern and Northern
667 Hemisphere at a 99% significance level. Quantification of the ozone recovery rate is largely
668 dependent on the parameterization for long term ozone variation, consistent with findings of
669 Kuttippurath et al. (2013). To determine which parameterization is more appropriate we compared
670 R^2 values for PHYS regression runs of section 3.3.1 in a similar manner as in Mäder et al. (2010)
671 which compares ozone regression performances using EESC or a linear function based on ozone
672 data obtained from ground-based observations. Results, shown in Figure 13, indicate that, among
673 the EESC variables with 3, 4 or 5.5 year air ages, the 3 year age-of-air EESC fits the ozone data
674 best. However, between 30°S and 80°S there exists a large region of higher performance with the
675 air age parameter set to 4 or 5.5 years. This may result from ozone not responding linearly to the EESC
676 in such a way that the fit to the 3 year air age EESC is better, even if the true age of air is higher. Looking

677 at a similar comparison now for the PWLT fits we note a clear distinction between high latitudes
678 (poleward of 50° N and 50° S) where the 1997-2010 ozone recovery period achieves high
679 performance and lower latitudes (equatorward of 50° N and 50° S) where the 2001-2010 ozone
680 recovery period fits best. This is unexpected since the higher age of air at high latitudes should
681 result in the turn-around point occurring later in time, whereas these results indicate the converse.
682 Finally, we see that the EESC long term ozone parameterization yields better performance at high
683 latitudes as compared to a PWLT function, which describes the long term ozone variation better at
684 lower latitudes. This result is caused by the fundamental difference of fitting a curve or a
685 piecewise linear function. At high latitudes, the larger age of air smooths the transition from ozone
686 depletion to ozone recovery resulting in a better fit using the EESC curve, whereas at low latitudes
687 the smaller age of air causes a more ad-hoc ozone turn around point, resulting in a better fit using a
688 PWLT function.

689 The recovery rates and trend uncertainties thus very much depend on the chosen regression
690 model and parameter settings of the EESC (age of air) and PWLT (recovery period). This indicates
691 that there is a considerable amount of uncertainty present in determining the ozone recovery rate.
692 Although these results suggest that the ozone layer is recovering globally as well as over the
693 Antarctic, care has to be taken as many uncertainties in both the data and methodology are not
694 taken into account. Based on these observations we conclude that ozone is recovering globally at a
695 rate between 0.2 and 1.7 DU/year and between 0.9 and 3.1 DU/year for the Antarctic ozone hole
696 period specifically. However, given the uncertainties discussed above it is not possible to
697 determine an appropriate trend uncertainty level, hence no statistical significance of the recovery
698 rates can be determined.

699

700 **5 Conclusions**

701

702 This study presents the first spatial multiple regression of 32 years of total ozone column data
703 based on assimilation of total ozone column measurements from satellites. A physically oriented
704 regression model (PHYS) forms the basis of the study, and is compared to a more statistically
705 oriented regression model (STAT). A second aim is the detection and quantification of ozone
706 recovery.

707 This first spatial regression study yields pronounced regional patterns in longitude and latitude
708 dimensions of ozone - regressor dependencies. The effect of ENSO on ozone is mainly identified
709 at the Pacific. We don't find clear indications of aerosol effects on ozone at the Antarctic. The
710 effect of the 11-year solar cycle appears to be more important in the Southern Hemisphere,
711 especially between -50° and 100° in longitudes, which is currently unexplained. And the effects
712 related to the southern polar vortex, clearly identified north of Antarctica, are large on total ozone
713 columns.

714 Our results broadly confirm findings from previous regression studies for local and zonal mean
715 total ozone records. A clear distinction exists between the tropics and higher latitudes. In the
716 tropics, ozone variability is dominated by the QBO whereas the 11-year solar cycle and ENSO
717 play minor roles. Outside of the tropics, effective chlorine loading is the most important factor,
718 and in the Northern Hemisphere volcanic aerosols also play a role. At mid-latitudes, dynamical
719 variability of the tropopause affects total ozone variability. For the Arctic, ozone variability is also
720 determined by the EP flux, which strongly affects the vortex stability. Over the Antarctic the EP-
721 flux is much less important.

722 The overall explanatory power of the PHYS model nears the explanatory power of the STAT
723 model (average R^2 values of 0.73 against 0.78 respectively for regressions south of 70°N). This
724 indicates a nearly complete characterization of seasonal variation in ozone in terms of physical
725 explanatory variables in the PHYS model. North of 70°N the explanatory power of the STAT
726 model is higher than that of the PHYS model.

727 As for post peak-EESC ozone trends, the results of our regressions indicate that standard
728 methods for determining trend uncertainties likely underestimate the true uncertainties in the
729 ozone trends that can be attributed to decreasing EESC. Hence, great care has to be taken with
730 discussing the statistical significance of these trends.

731 Ongoing research will focus on these unexplained variations by examining the regression
732 residuals. In addition, effort will be put into investigating uncertainties in both regressors – what is
733 the uncertainty in the regressors and how sensitive are the regressions to these uncertainties – and
734 the measurement errors of ozone. Furthermore, we also plan to perform other regression analyses
735 to further examine the robustness of our results. Finally, robustness of the results will be tested by
736 extending the MSR ozone record forward and backward in time.

737

738 **Acknowledgements**

739

740 The authors thank Mathisca de Gunst from the Free University of Amsterdam and Piet
741 Stammes from the KNMI for their useful comments and suggestions. Furthermore, we would like
742 to thank three anonymous reviewers for their useful suggestions on improving this manuscript.

743 **References**

744

745 Allaart, M. A. F., Kelder, H., and Heijboer, L. C.: On the relation between ozone and potential
746 vorticity, *Geophys. Res. Lett.*, 20, 811–814, 1993.

747

748 Baldwin, M. P., Gray, L. J., Dunkerton, T. J., Hamilton, K., Haynes, P. H., Randel, W. J.,
749 Holton, J. R., Alexander, M. J., Hirota, I., Horinouchi, T., Jones, D. B. A., Kinnersley, J. S.,
750 Marquardt, C., Sato, K., and Takahashi, M. G. L.: The quasi-biennial oscillation, *Rev. Geophys.*,
751 39, 179–229, 2001.

752

753 Bodeker, G. E., Boyd, I. S., and Matthews, W. A.: Trends and variability in vertical ozone and
754 temperature profiles measured by ozonesondes at Lauder, New Zealand: 1986–1996, *J. Geophys.*
755 *Res.*, 103, 661–681, 1998.

756

757 Bodeker, G. E., Scott, J. C., Kreher, K., and McKenzie, R. L.: Global ozone trends in potential
758 vorticity coordinates using TOMS and GOME intercompared against the Dobson network:
759 1978–1998, *J. Geophys. Res.*, 106, 29–42, 2001.

760

761 Bourassa, A. E., Robock, A., Randel, W. J., Deshler, T., Rieger, L. A., Lloyd, N. D., Llewellyn, E.
762 J., and Degenstein, D. A.: Large volcanic aerosol load in the stratosphere linked to Asian
763 monsoon transport, *Science*, 337, 78–81, 2012.

764

765 Braesicke, P., Brühl, C., Dameris, M., Deckert, R., Eyring, V., Giorgetta, M. A., Mancini, E.,

766 Manzini, E., Pitari, G., Pyle, J. A., and Steil, B.: A model intercomparison analysing the link
767 between column ozone and geopotential height anomalies in January, *Atmos. Chem. Phys.*, 8,
768 2519–2535, doi:10.5194/acp-8-2519-2008, 2008.

769

770 Brunner, D., Staehelin, J., Maeder, J. A., Wohltmann, I., and Bodeker, G. E.: Variability and
771 trends in total and vertically resolved stratospheric ozone based on the CATO ozone data
772 set, *Atmos. Chem. Phys.*, 6, 4985–5008, doi:10.5194/acp-6-4985-2006, 2006.

773

774 de Laat, A. T. J. and van Wheel, M.: The 2010 Antarctic ozone hole: observed reduction in ozone
775 destruction by minor sudden stratospheric warmings, *Scientific Reports*, 1, 38,
776 doi:10.1038/srep00038, 2010.

777

778 Deshler, T., Adriani, A., Gobbi, G. P., Hofmann, D. J., Di Donfrancesco, G., and Johnson, B. J.:
779 Volcanic aerosol and ozone depletion within the antarctic polar vortex during the austral
780 spring of 1991, *Geophys. Res. Lett.*, 19, 1819–1822, 1992.

781

782 Douglass, A., Fioletov, V., Godin-Beekman, S., Müller, R., Stolarski, R. S., Webb, A., Arola, A.,
783 Burkholder, J. B., Burrows, J. P., Chipperfield, M. P., Cordero, R., David, C., den Outer, P. N.,
784 Diaz, S. B., Flynn, L. E., Hegglin, M., Herman, J. R., Huck, P., Janjai, S., Jánosi, L. M., Krzyscin,
785 J. W., Liu, Y., Logan, J., Matthes, K., McKenzie, R. L., Muthama, N. J., Petropavlovshikh, I.,
786 Pitts, M., Ramachandran, S., Rex, M., Salawitch, R. J., Sinnhuber, B.-M., Staehelin, J., Strahan,
787 S., Tourpali, K., Valverde-Canossa, J., Vigouroux, C.: Stratospheric ozone and surface ultraviolet

788 radiation, CH 2 in Scientific assessment of ozone depletion: 2010, WMO Glob. Ozone Res. And
789 Mon. Proj., Report No. 52, 516 pp., Geneva, Switzerland, 2011.

790
791 Eskes, H. J., van der A, R. J., Brinksma, E. J., Veefkind, J. P., de Haan, J. F., and Valks, P. J. M.:
792 Retrieval and validation of ozone columns derived from measurements of SCIAMACHY on
793 Envisat, Atmos. Chem. Phys. Discuss., 5, 4429–4475, doi:10.5194/acpd-5-4429-2005,
794 2005.

795
796 Fioletov, V. E.: Ozone climatology, trends, and substances that control ozone, Atmos. Ocean,
797 46, 39–67, doi:10.3137/ao.460103, 2008.

798
799 Fortuin, J. P. F. and Kelder, H.: An ozone climatology base on ozonesonde and satellite
800 measurements, J. Geophys. Res., 103, 31709–31734, 1998.

801
802 Frohlich, C.: Observations of irradiance variations, Space Sci. Rev., 94, 15–24, 2000.

803
804 Hansen, G. and Svenøe, T.: Multilinear regression analysis of the 65 year Tromsø total ozone
805 series, J. Geophys. Res., 110, D10103, doi:10.1029/2004JD005387, 2005.

806
807 Harris, N. R. P., Kyrö, E., Staehelin, J., Brunner, D., Andersen, S.-B., Godin-Beekman, S.,
808 Dhomse, S., Hadjinicolaou, P., Hansen, G., Isaksen, I., Jrrar, A., Karpetchko, A., Kivi, R.,
809 Knudsen, B., Krizan, P., Lastovicka, J., Maeder, J., Orsolini, Y., Pyle, J. A., Rex, M., Vanicek, K.,
810 Weber, M., Wohltman, I., Zanis, P., and Zerefos, C.: Ozone trends at northern mid- and high

811 latitudes - a European perspective, *Ann. Geophys.*, 26, 1207-1220, doi:10.5194/angeo-26-1207-
812 2008, 2008.

813

814 Hassler, B., Bodeker, G. E., Solomon, S., and Young, P. J.: Changes in the polar vortex: effects
815 on Antarctic total ozone observations at various stations, *Geophys. Res. Lett.*, 38, L01805,
816 doi:10.1029/2010GL045542, 2011.

817

818 Hofmann, D. J. and Oltmans, S. J.: Anomalous Antarctic ozone during 1992: evidence for
819 Pinatubo volcanic aerosol effects, *J. Geophys. Res.*, 98, 18555–18561, doi:10.1029/93JD02092,
820 1993.

821

822 Hofmann, D. J., Oltmans, S. J., Harris, J. M., Johnson, B. J., and Lathrop, J. A.: Ten years of
823 ozonesonde measurements at the south pole: implications for recovery of springtime Antarctic
824 ozone, *J. Geophys. Res.*, 102, 8931–8943, doi:10.1029/96JD03749, 1997.

825

826 Hood, L. L. and Soukharev, B. E.: Interannual variations of total ozone at northern midlatitudes
827 correlated with stratospheric EP flux and potential vorticity, *J. Atmos. Sci.*, 62, 3724–3740,
828 doi:10.1175/JAS3559.1, 2005.

829

830 Hurwitz, M. M. and Newman, P. A.: 21st century trends in Antarctic temperature and Polar
831 Stratospheric Cloud (PSC) area in the GEOS chemistry-climate model, *J. Geophys. Res.*,
832 115, D19109, doi:10.1029/2009JD013397, 2010.

833

834 Jones, A., Urban, J., Murtagh, D. P., Eriksson, P., Brohede, S., Haley, C., Degenstein, D.,
835 Bourassa, A., von Savigny, C., Sonkaew, T., Rozanov, A., Bovensmann, H., and Burrows, J.:
836 Evolution of stratospheric ozone and water vapour time series studied with satellite measurements,
837 *Atmos. Chem. Phys.*, 9, 6055–6075, doi:10.5194/acp-9-6055-2009, 2009.

838

839 Kanamitsu, M., Ebisuzaki, W., Woollen, J., Yang, S. K., Hnilo, J. J., Fiorino, M., and Potter, G. L.:
840 NCEP-DOE AMIP-11 REANALYSIS (R-2), *B. Am. Meteorol. Soc.*, 83, 1631–1643, 2006.

841

842 Kieseewetter, G., Sinnhuber, B.-M., Weber, M., and Burrows, J. P.: Attribution of stratospheric
843 ozone trends to chemistry and transport: a modelling study, *Atmos. Chem. Phys.*, 10, 12073-2010,
844 2010.

845

846 Knight, J. R., Austin, J., Grainger, R. G., and Lambert, A.: A three-dimensional model simulation
847 of the impact of Mt. Pinatubo aerosol on the Antarctic ozone hole, *Q. J. Roy. Meteor. Soc.*,
848 124, 1527–1558, doi:10.1002/qj.49712454909, 1998.

849

850 Kuttippurath, J., Lefèvre, F., Pommereau, J.-P., Roscoe, H. K., Goutail, F., Pazmiño, A., and
851 Shanklin, J. D.: Antarctic ozone loss in 1979–2010: first sign of ozone recovery, *Atmos.*
852 *Chem. Phys.*, 13, 1625–1635, doi:10.5194/acp-13-1625-2013, 2013.

853

854 Lean, J.: Contribution of ultraviolet irradiance variations to changes in the sun’s total irradiance,
855 *Science* 244, 197–200, doi:10.1126/science.244.4901.197, 1989.

856

857 Li, F.: Interactive comment on “stratospheric ozone in post-CFC era” by Li, F. et al., Atmos.
858 Chem. Phys. Discuss., 8, S11413–S11416, 2009.

859

860 Mäder, J. A., Staehelin, J., Brunner, D., Stahel, W. A., Wohltmann, I., and Peter, T.: Statistical
861 modeling of total ozone: selection of appropriate explanatory variables, J. Geophys. Res.,
862 112, D11108, doi:10.1029/2006JD007694, 2007.

863

864 Mäder, J. A., Staehelin, J., Peter, T., Brunner, D., Rieder, H. E., and Stahel, W. A.: Evidence for
865 the effectiveness of the Montreal Protocol to protect the ozone layer, Atmos. Chem. Phys.,
866 10, 12161–12171, doi:10.5194/acp-10-12161-2010, 2010.

867

868 McCormack, J. P., Siskind, D. E., and Hood, L. L.: Solar-QBO interaction and its impact on
869 stratospheric ozone in a zonally averaged photochemical transport model of the middle
870 atmosphere, J. Geophys. Res., 112, D16109, doi:10.1029/2006JD008369, 2007.

871

872 Miyazaki, K., Iwasaki, T., Shibata, K., and Deushi, M.: Roles of transport in the seasonal variation
873 of the total ozone amount, J. Geophys. Res., 110, D18309, doi:10.1029/2005JD005900, 2005.

874

875 Molina, M. J. and Rowland, F. S.: Stratospheric sink for chlorofluoromethanes: chlorine atom-
876 catalysed destruction of ozone, Nature, 249, 810–812; doi:10.1038/249810a0, 1974.

877

878 Newman, P. A., Gleason, J. F., McPeters, R. D., and Stolarski, R. S.: Anomalously low ozone
879 over the Arctic, Geophys. Res. Lett., 24, 2689–2692, 1997.

880
881 Newman, P. A., Nash, E. R., Kawa, S. R., Montzka, S. A., and Schauffler, S. M.: When will the
882 Antarctic ozone hole recover?, *Geophys. Res. Lett.*, 33, L12814, doi:10.1029/2005GL025232,
883 2006.
884
885 Ohring, G. and Muench, H. S.: relationships between ozone and meteorological parameters in the
886 lower stratosphere, *J. Meteor.*, 17, 195–206, doi:10.1175/1520-
887 0469(1960)017<0195:RBOAMP>2.0.CO;2, 1960.
888
889 Pan, L. L., Kunz, A., Homeyer, C. R., Munchak, L. A., Kinnison, D. E., and Tilmes, S.:
890 Commentary on using equivalent latitude in the upper troposphere and lower stratosphere, *Atmos.*
891 *Chem. Phys.*, 12, 9187–9199, doi:10.5194/acp-12-9187-2012, 2012.
892
893 Press, W. H., Flannery, B. P., Teukolski, S. A., and Vetterling, W. T. (Eds): *Numerical Recipes*,
894 Cambridge University Press, Cambridge, UK, 504-508, 1989.
895
896 Randel, W. J., Wu, F., and Stolarski, R.: Changes in Column Ozone Correlated with the
897 Stratospheric EP Flux, *J. Meteorol. Soc. Jpn.*, 80, 849–862, 2002.
898
899 Randel, W. J., Garcia, R. R., Calvo, N., and Marsh, D.: ENSO influence on zonal mean
900 temperature and ozone in the tropical lower stratosphere, *Geophys. Res. Lett.*, 36, L15822,
901 doi:10.1029/2009GL039343, 2009.
902

903 Rieder, H. E., Staehelin, J., Maeder, J. A., Peter, T., Ribatet, M., Davison, A. C., Stübi, R., Weihs,
904 P., and Holawe, F.: Extreme events in total ozone over Arosa - Part 2: Fingerprints of atmospheric
905 dynamics and chemistry and effects on mean values and long-term changes, *Atmos. Chem. Phys.*,
906 10, 10033-10045, doi:10.5194/acp-10-10033-2010, 2010.

907

908 Riishøjgaard, J. P. and Källén, E.: On the correlation between ozone and potential vorticity for
909 large scale Rossby waves, *J. Geophys. Res.*, 102, 8793–8804, 1997.

910

911 Robock, A., Adams, T., Moore, M., Oman, L., and Stenchikov, G.: Southern Hemisphere
912 atmospheric circulation effects of the 1991 Mount Pinatubo eruption, *Geophys. Res. Lett.*, 34,
913 L23710, doi:10.1029/2007GL031403, 2007.

914

915 Rozanov, E. V., Schlesinger, M. E., Andronova, N. G., Yang, F., Malyshev, S. L., Zubov, V. A.,
916 Egorova, T. A., and Li, B.: Climate/chemistry effects of the Pinatubo volcanic eruption simulated
917 by the UIUC stratosphere/troposphere GCM with interactive photochemistry, *J. Geophys.*
918 *Res.*, 107, 4594, doi:10.1029/2001JD000974, 2002.

919

920 Salby, M. J., Titova, E. A., and Deschamps, L.: Changes of the Antarctic ozone hole: controlling
921 mechanisms, seasonal predictability, and evolution, *J. Geophys. Res.*, 117, D10111,
922 doi:10.1029/2011JD016285, 2012.

923

924 Sato, M., Hansen, J. E., McCormick, M. P., and Pollack, J. B.: Stratospheric aerosol optical
925 depth, 1850–1990, *J. Geophys. Res.*, 98, 22987–22994, 1993.

926
927 Shindell, D. T., Rind, D., Balachandran, N., Lean, J., and Lonergan, P.: Solar cycle variability,
928 ozone and climate, *Science*, 284, 305–308, 1999.

929
930 Solomon, S., Portmann, R. W., Garcia, R. R., Thomason, L. W., Poole, L. R., and Mc-
931 Cormick, M. P.: The role of aerosol variations in anthropogenic ozone depletion at northern
932 midlatitudes, *J. Geophys. Res.*, 101, 6713–6727, doi:10.1029/95JD03353, 1996.

933
934 Solomon, S., Daniel, J. S., Neely III, R. R., Vernier, J.-P., Dutton, E. G., and Thomason, L. W.:
935 The persistently variable “background” stratospheric aerosol layer and global climate change,
936 *Science*, 333, 866–870, 6044, doi:10.1126/science.1206027, 2012.

937
938 Soukharev, B. E. and Hood, L. L.: Solar cycle variation of stratospheric ozone: Multiple regression
939 nalysis of long-term satellite data sets and comparisons with models, *J. Geophys. Res.*, 111,
940 D20314, doi:10.1029/2006JD007107, 2006.

941
942 Stiller, G.P., von Clarmann, T., Haenel, F., Funke, B., Glatthor, N., Grabowski, U., Kellmann, S.,
943 Kiefer, M., Linden, A., Lossow, S., and Lopez-Puertas, M.: Observed temporal evolution of global
944 mean age of stratospheric air for 2002 to 2010 period, *Atmos. Chem. Phys.*, 12, 3311-3331,
945 doi:10.5194/acp-12-3311-2012, 2012.

946
947 Stolarski, R. S. and Cicerone, R. J.: Stratospheric chlorine: a possible sink for ozone, *Can. J.*
948 *Chem.*, 52, 1610, 1974.

949
950 Stolarski, R. S., Bloomfield, P., and McPeters, R. D.: Total ozone trends deduced from NIMBUS
951 7 TOMS data, *Geophys. Res. Lett.*, 18, 1015–1018, 1991.
952
953 Valis, G. K.: *Atmospheric and Oceanic Fluid Dynamics: Fundamentals and Large-Scale*
954 *Circulation*, ISBN 0-5218-4969-1, Cambridge University Press, New York, USA, 768 pp., 2007.
955
956 van der A, R. J., Allaart, M. A. F., and Eskes, H. J.: Multi sensor reanalysis of total ozone,
957 *Atmos. Chem. Phys.*, 10, 11277–11294, doi:10.5194/acp-10-11277-2010, 2010.
958
959 Vernier, J.-P., Thomason, L. W., Pommereau, J.-P., Bourassa, A., Pelon, J., Garnier, A.,
960 Hauchecorne, A., Blanot, L., Trepte, C., Degenstein, D., and Vargas, F.: Major influence of
961 tropical volcanic eruptions on the stratospheric aerosol layer during the last decade, *Geophys.*
962 *Res. Lett.*, 38, L12807, doi:10.1029/2011GL047563, 2011.
963
964 Weatherhead, E. C. and Andersen, S. B.: The search for signs of recovery of the ozone layer,
965 *Nature*, 441, 39–45, doi:10.1038/nature04746, 2006.
966
967 Weber, M., Dikty, S., Burrows, J. P., Garny, H., Dameris, M., Kubin, A., Abalichin, J., and
968 Langematz, U.: The Brewer-Dobson circulation and total ozone from seasonal to decadal time
969 scales, *Atmos. Chem. Phys.*, 11, 11221–11235, doi:10.5194/acp-11-11221-2011, 2011.
970
971 Witte, J. C., Schoeberl, M. R., Douglass, A. R., and Thompson, A. M.: The Quasi-biennial

972 Oscillation and annual variations in tropical ozone from SHADOZ and HALOE, *Atmos. Chem.*
973 *Phys.*, 8, 3929–3936, doi:10.5194/acp-8-3929-2008, 2008.

974

975 Wolter, K. and Timlim, M. S.: Monitoring ENSO in COADS with a seasonally adjusted principal
976 component index, *Proc. Of the 7th Climate Diagnostics Workshop*, 01/1993, Norman,
977 Oklahoma, 52–57, 1993.

978

979 Wolter, K. and Timlim, M. S.: Measuring the strength of ENSO events – how does 1997/98
980 rank?, *Weather*, 53, 315–324, 1998.

981

982 WMO: Scientific assessment of ozone depletion: 2010, *WMO Glob. Ozone Res. And Mon.*
983 *Proj.*, Report No. 52, 516 pp., Geneva, Switzerland, 2011.

984

985 Wohltmann, I., Lehmann, R., Rex, M., Brunner, D., and Mader, J. A.: A process-oriented
986 regression model for column ozone, *J. Geophys. Res.*, 112, D12304, doi:10.1029/2006JD007573,
987 2007.

988

989 Yang, H. and Tung, K. K.: On the phase propagation of extratropical ozone quasi-biennial
990 oscillation in observational data, *J. Geophys. Res.*, 100, 9091–9100, doi:10.1029/95JD00694,
991 1995.

992

993 Ziemke, J. R., Chandra, S., Oman, L. D., and Bhartia, P. K.: A new ENSO index derived
994 from satellite measurements of column ozone, *Atmos. Chem. Phys.*, 10, 3711–3721,

995 doi:10.5194/acp-10-3711-2010, 2010.

996

997

998

999

1000

1001

| Proxy | Data description | Source |
|----------------|---|---|
| O ₃ | Globally gridded (1x1.5 degrees) ozone in DU | www.temis.nl/protocols/O3global.html |
| SOLAR | The 10.7cm Solar Flux | ftp://ftp.ngdc.noaa.gov/STP/space-weather/solar-data/solar-features/solar-radio/noontime-flux/penticton/penticton_adjusted/listings/ |
| EESC | Effective stratospheric chlorine and bromine | Acd-ext.gsfc.nasa.gov/Data_services/automailer/index.html |
| AERO | 7.5 degree zonal bands of Aerosols Optical Thickness. | Data.giss.nasa.gov/modelforce/strataer/tau_map.txt . |
| EP | Vertical EP-flux at 100 hPa averaged over 45-90 degrees North [N] and South [S] | www.esrl.noaa.gov/psd/data/gridded/data.ncep.reanalysis2.html |
| QBO | QBO index at several pressure levels | www.geo.fu-berlin.de/en/met/ag/strat/produkte/qbo/ |
| ENSO | Multivariate El Nino Southern Oscillation index | www.esrl.noaa.gov/psd/enso/mei |
| GEO | Geopotential height at the 500 hPa level (gridded) | Data-portal.ecmwf.int/data/d/interim_moda/levtype=pl/ |
| PV | Potential Vorticity at 150 hPa level (gridded) | Data-portal.ecmwf.int/data/d/interim_moda/levtype=pl/ |
| DAY | Average day length (gridded) | Calculated based on geometric variations |

1002

1003 **Table 1.** List of variables and their sources.

1004

| Proxy | SOLAR | EESC | AERO | EP-N | EP-S | QBO10 | QBO30 | ENSO |
|-------|-------|-------|-------|--------------|--------------|-------|-------|-------|
| SOLAR | 1.00 | -0.29 | 0.18 | 0.04 | -0.09 | 0.01 | 0.03 | 0.04 |
| EESC | -0.29 | 1.00 | -0.22 | 0.02 | 0.18 | 0.03 | 0.01 | -0.12 |
| AERO | 0.18 | -0.22 | 1.00 | 0.01 | 0.11 | 0.13 | -0.13 | 0.29 |
| EP-N | 0.04 | 0.02 | 0.01 | 1.00 | -0.52 | 0.03 | 0.14 | -0.05 |
| EP-S | -0.09 | 0.18 | 0.11 | -0.52 | 1.00 | 0.05 | -0.18 | 0.01 |
| QBO10 | 0.01 | 0.03 | 0.13 | 0.03 | 0.05 | 1.00 | 0.03 | -0.02 |
| QBO30 | 0.03 | 0.01 | -0.03 | 0.14 | -0.18 | 0.03 | 1.00 | 0.04 |
| ENSO | 0.04 | -0.12 | 0.29 | -0.05 | 0.01 | -0.02 | 0.04 | 1.00 |

1005

1006 **Table 2.** Table of correlations for non-gridded proxies. Due to high correlation values between
1007 EP-N and EP-S, these variables are only used in the Northern and Southern Hemisphere,
1008 respectively. QBO10 and QBO30 represent the QBO index at 10 and at 30 hPa, respectively.

1009

| Model Variables | Intercept | Group A | Group B | Fourier terms |
|-----------------|-----------|----------|--------------|---------------|
| PHYS model | included | included | included | not included |
| STAT model | included | included | not included | included |

1010

1011 **Table 3:** Overview of variables included in the regression models with “group A” consisting of
1012 EESC, SOLAR, AERO, ENSO and their corresponding alternative explanatory variables, “group
1013 B” consisting of DAY, EP, PV and GEO and “Fourier terms” consisting of sines and cosines with
1014 periods of a year and half a year.

1015

| PHYS model at Reykjavik | | | STAT model at Reykjavik | | |
|-------------------------|-------------|-----------|-----------------------------|-------------|-----------|
| Variable | Coefficient | St. Error | Variable | Coefficient | St. Error |
| Intercept | 339.27 | 1.07 | Intercept | 339.7 | 0.98 |
| EP | 34.51 | 2.26 | Sine (annual cycle) | 43.7 | 1.41 |
| GEO | -23.77 | 2.22 | Cosine (annual cycle) | -20.7 | 1.29 |
| PV | 3.87 | 1.31 | Cosine (half | -8.5 | 1.32 |

| | | | | | |
|------|-------|------|-------------|------|------|
| | | | year cycle) | | |
| DAY | 51.02 | 1.84 | QBO30 | -3.6 | 1.01 |
| EESC | -4.62 | 1.03 | QBO30_2 | -2.7 | 0.97 |
| | | | QBO10 | 3.3 | 0.92 |
| | | | EESC | -4.5 | 0.90 |
| | | | AERO | -2.4 | 0.92 |

1016

1017 **Table 4.** Regression coefficients and standard errors of regressions at Reykjavik, Iceland. QBO10
 1018 and QBO30 represent the QBO index at 10 and at 30 hPa, respectively.

1019

| PHYS model at Bogota | | | STAT model at Bogota | | |
|----------------------|-------------|-----------|-----------------------------|-------------|-----------|
| Variable | Coefficient | St. Error | Variable | Coefficient | St. Error |
| Intercept | 254.08 | 0.34 | Intercept | 254.0 | 0.25 |
| EP | -8.10 | 0.33 | Sine (annual cycle) | -10.1 | 0.36 |
| GEO | -1.06 | 0.41 | Cosine (annual cycle) | -7.6 | 0.35 |
| ENSO | -1.35 | 0.41 | Cosine (half year cycle) | -4.1 | 0.35 |
| QBO30 | 5.26 | 0.34 | ENSO | -1.5 | 0.27 |
| QBO10 | 2.67 | 0.34 | ENSO_2 | -1.0 | 0.26 |
| | | | QBO30 | 5.5 | 0.26 |
| | | | QBO10 | 2.9 | 0.25 |

1020

1021 **Table 5.** Regression coefficients and standard errors of regressions at Bogota, Colombia. QBO10
 1022 and QBO30 represent the QBO index at 10 and at 30 hPa, respectively.

1023

| PHYS model at Antarctica | | | STAT model at Antarctica | | |
|--------------------------|-------------|-----------|--------------------------|-------------|-----------|
| Variable | Coefficient | St. Error | Variable | Coefficient | St. Error |
| Intercept | 240.6 | 1.25 | Intercept | 242.0 | 1.16 |
| EP | -6.0 | 2.08 | Sine (annual | 29.7 | 1.85 |

| | | | | | |
|--------|-------|------|--------------------------|------|------|
| | | | cycle) | | |
| PV | -20.6 | 1.86 | Sine (half year cycle) | 22.3 | 1.67 |
| SOLAR | 3.38 | 1.3 | Cosine (annual cycle) | -8.3 | 2.23 |
| EESC | -6.07 | 1.26 | Cosine (half year cycle) | 20.8 | 1.78 |
| EESC_2 | 24.9 | 1.53 | EESC | -9.4 | 1.16 |
| | | | EESC_2 | 11.3 | 1.79 |
| | | | SOLAR | 3.1 | 1.20 |

1024

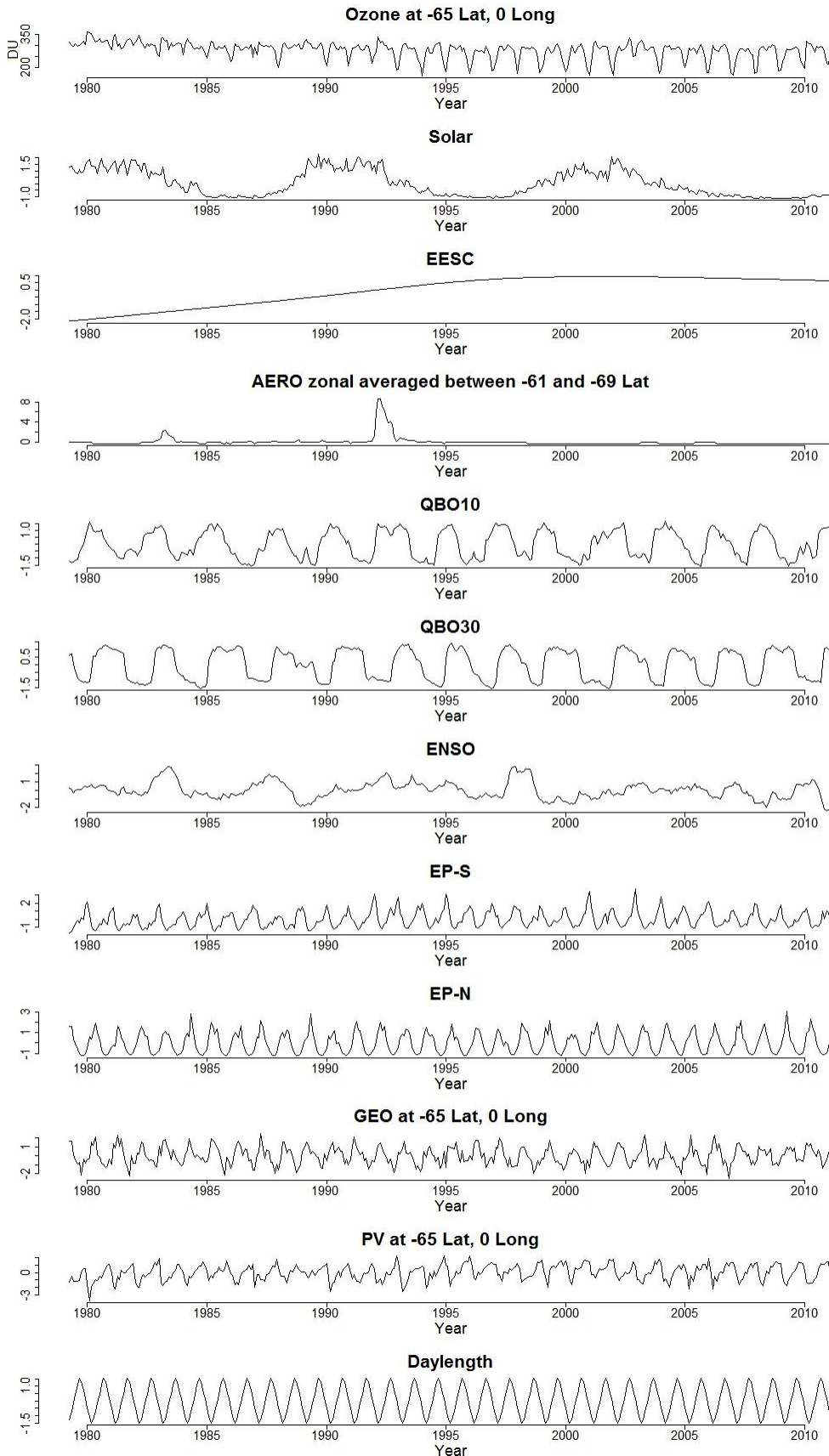
1025 **Table 6.** Regression coefficients and standard errors of regressions at 80°S, 0°E (Antarctica).

1026

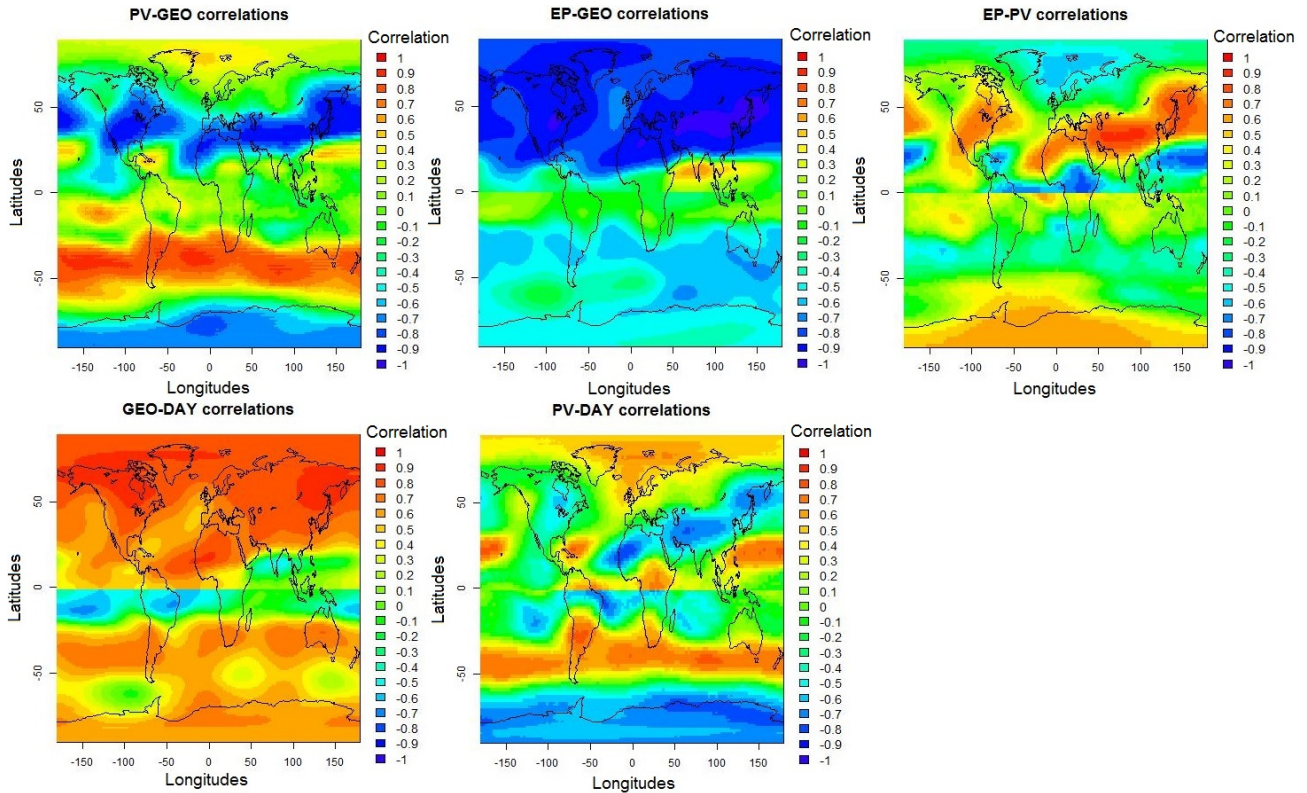
| Trend method | Age of air (EESC) Rec. period (PWLT) | NH | SH | Antarctic |
|--------------|---|------------|------------|------------|
| EESC | 3 | 0.6 ± 0.14 | 0.7 ± 0.22 | 1.8 ± 0.22 |
| | 4 | 0.4 ± 0.11 | 0.5 ± 0.17 | 1.4 ± 0.18 |
| | 5.5 | 0.2 ± 0.07 | 0.3 ± 0.13 | 0.9 ± 0.14 |
| PWLT | 1997-2010 | 1.0 ± 0.73 | 0.7 ± 1.59 | 1.3 ± 4.8 |
| | 1999-2010 | 1.3 ± 0.77 | 1.0 ± 1.70 | 2.3 ± 4.6 |
| | 2001-2010 | 1.7 ± 0.88 | 1.4 ± 1.81 | 3.1 ± 5.8 |

1027 **Table 7.** Average ozone recovery rates based on EESC and PWLT regression estimates
1028 representative for the PHYS model. Values are in DU/year, uncertainties indicate the 2σ (95%)
1029 confidence intervals. The EESC-based trend estimates are determined for three different values for

1030 the EESC age-of-air, the PWLT estimates are provided for three different time periods.

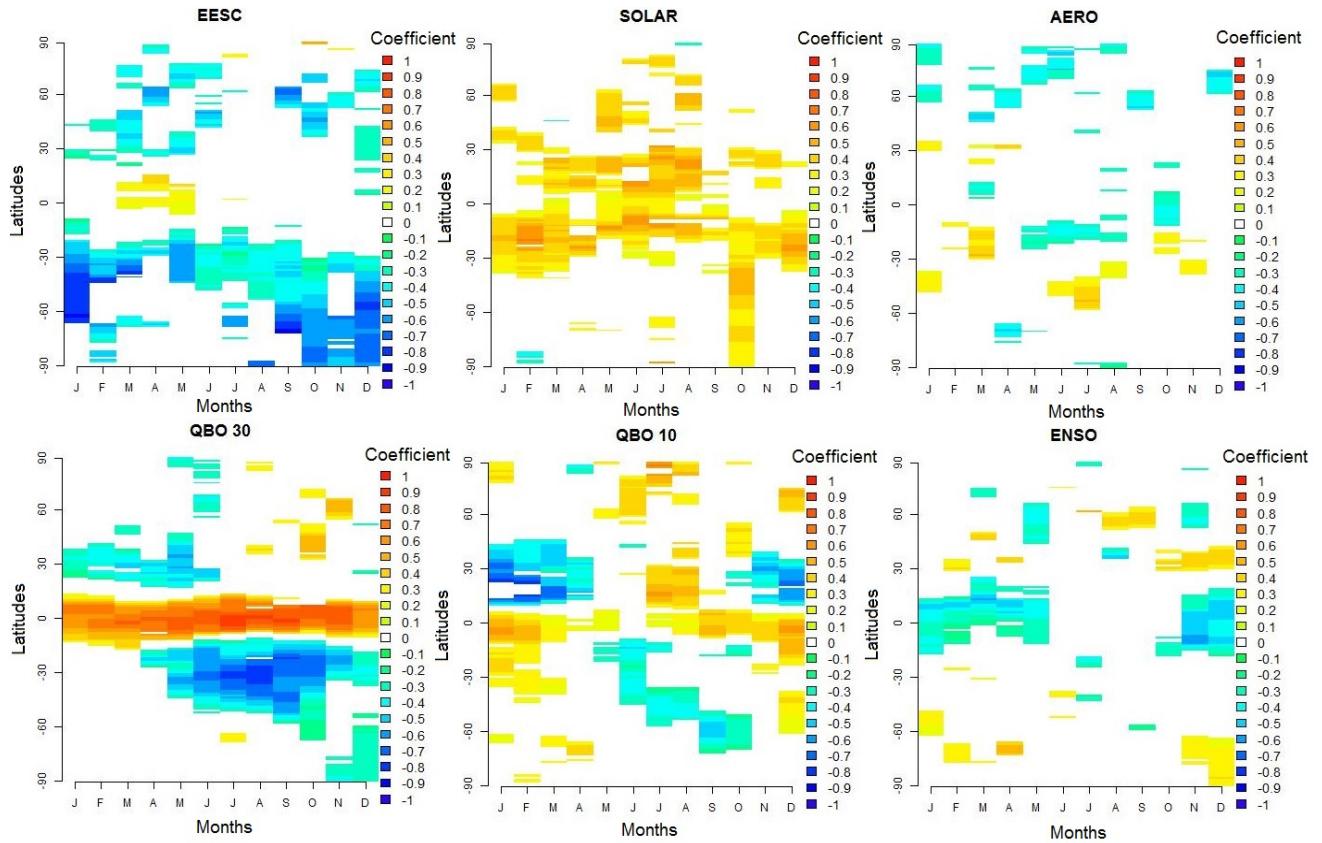


1032 **Figure 1.** Time series of ozone and explanatory variables for the period 1979-2010 at 65°S and
 1033 0°E. The explanatory variables are normalized prior to plotting. QBO10 and QBO30 represent the
 1034 QBO index at 10 and at 30 hPa, respectively.



1035
 1036 **Figure 2.** Correlation values between EP, GEO, PV and DAY. The correlations between EP and
 1037 DAY are left out, since these values are nearly constant throughout both hemispheres (0.17 in SH
 1038 and -0.69 in NH).

1039

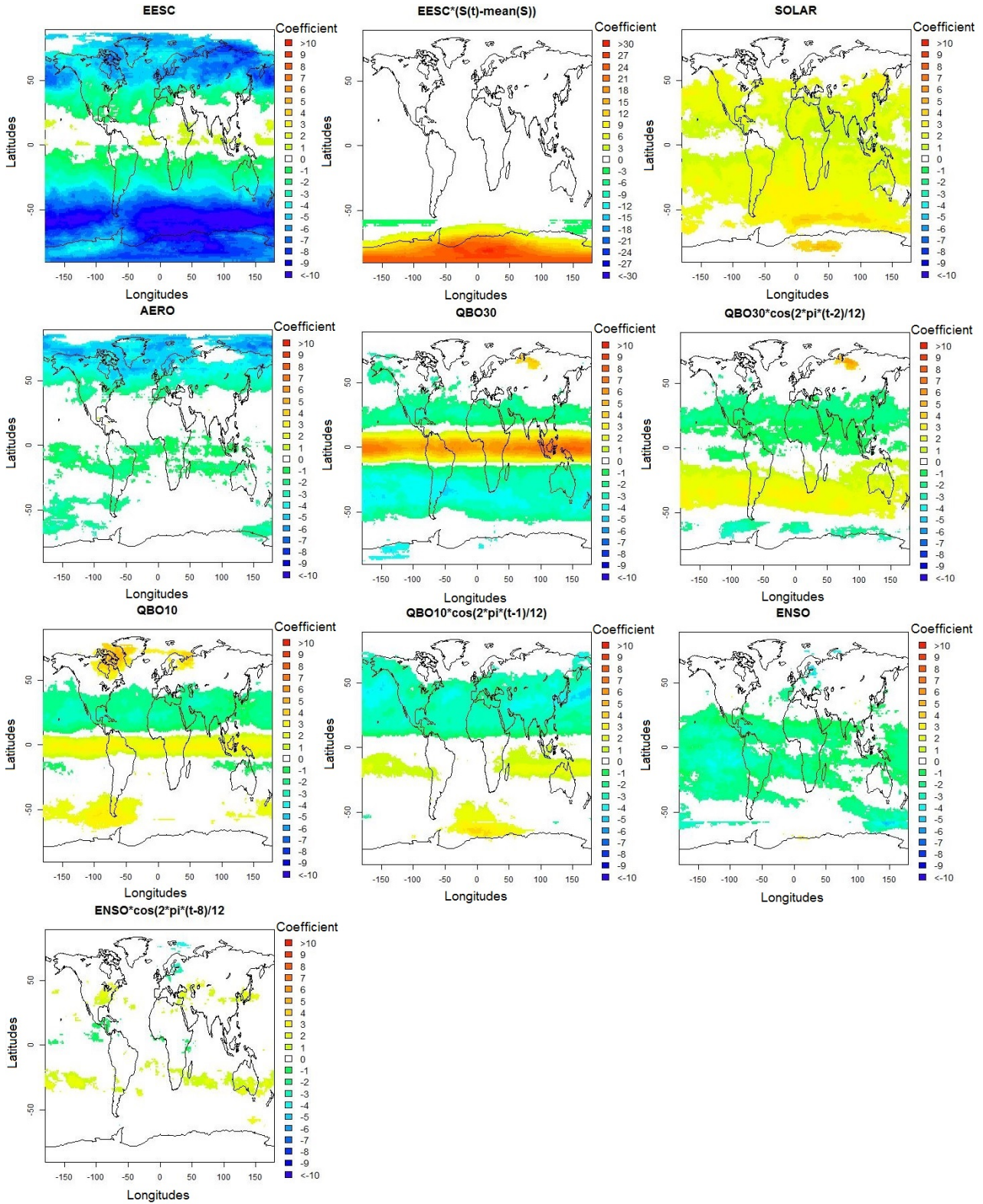


1040

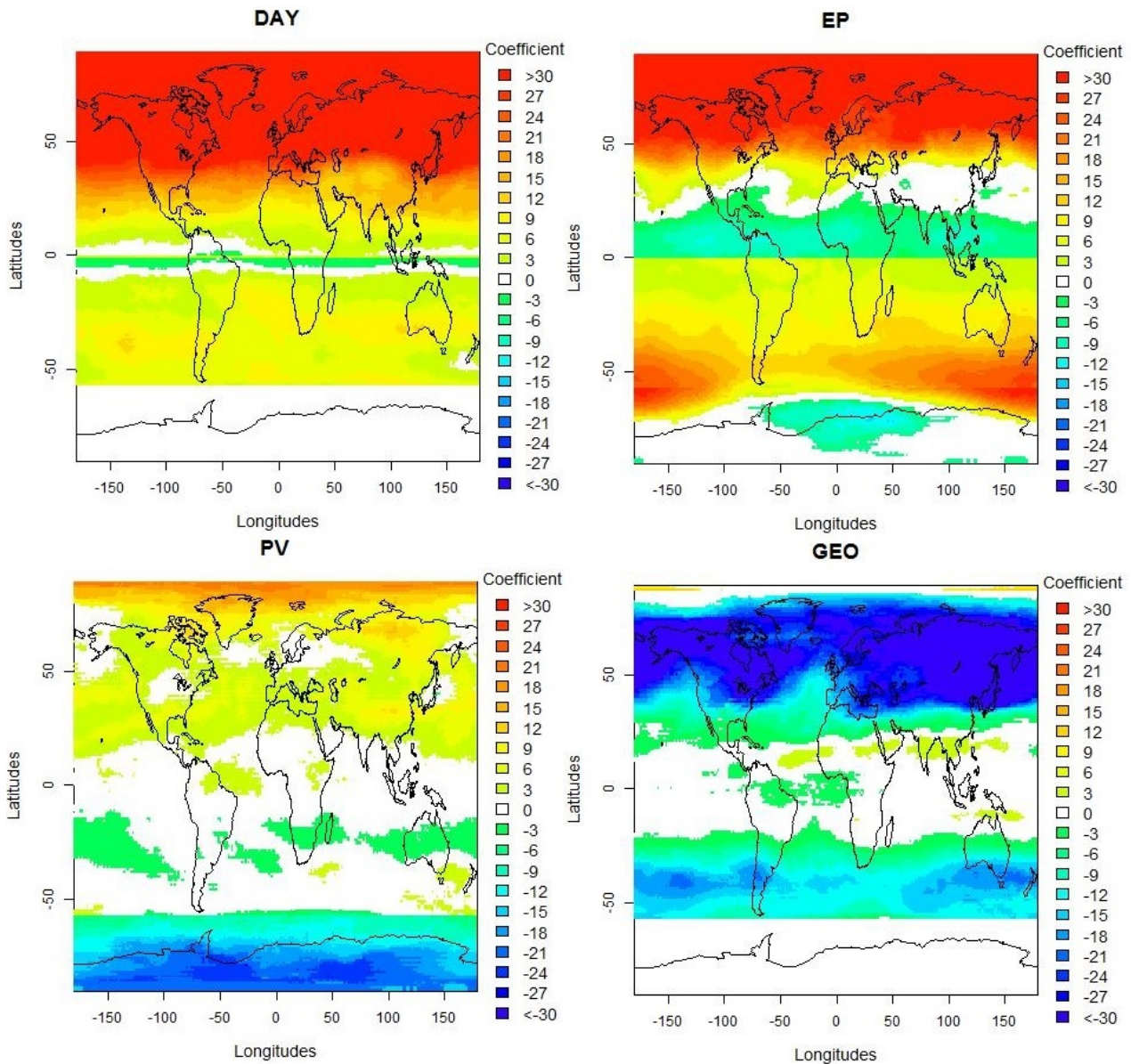
1041 **Figure 3.** Monthly regression coefficient estimates for the non-seasonal explanatory variables.

1042 White regions indicate non-significant coefficient estimates at the 90% confidence level. QBO10

1043 and QBO30 represent the QBO index at 10 and at 30 hPa, respectively.

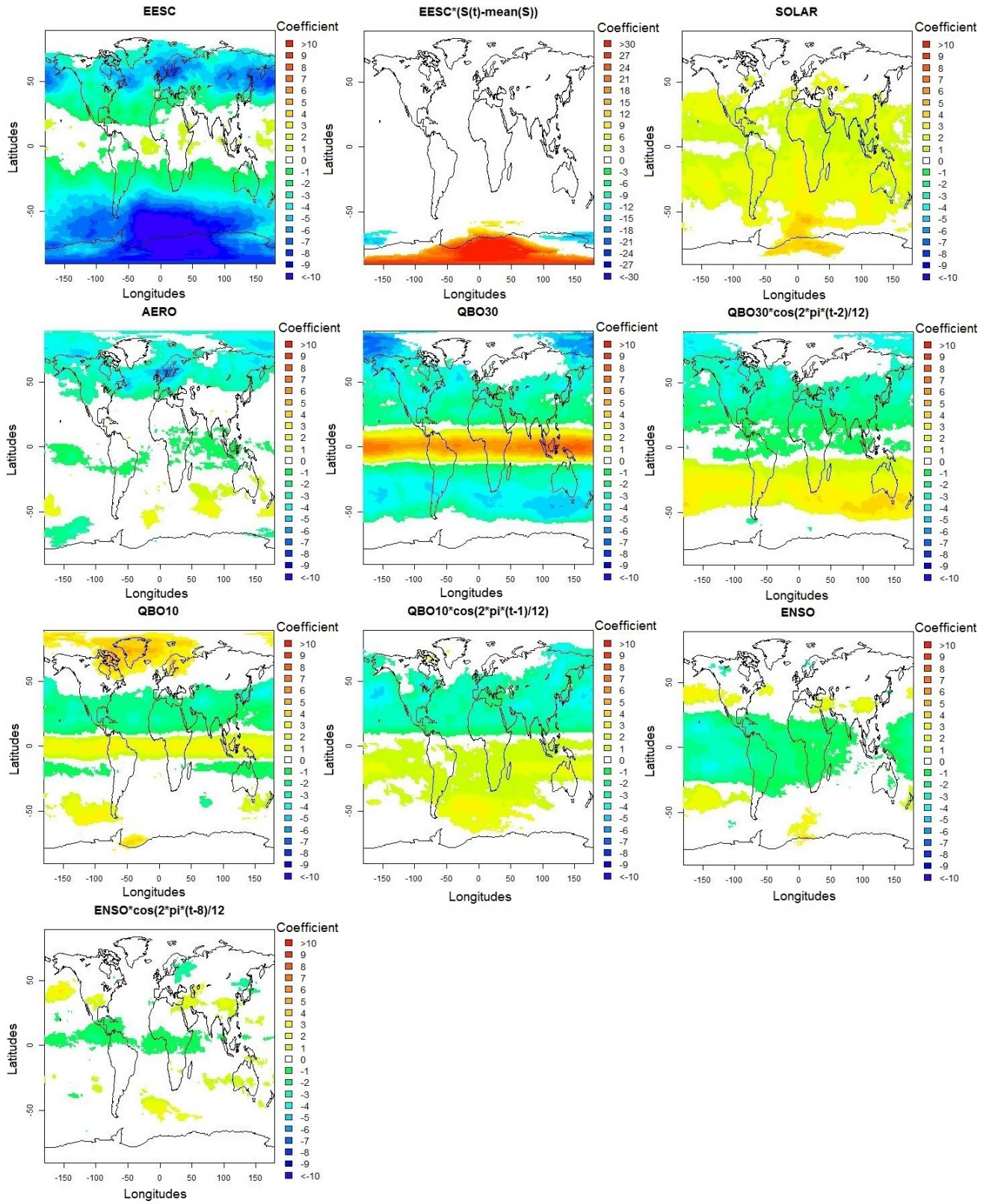


1045 **Figure 4.** Regression coefficient estimates of non-seasonal variables for the PHYS model on a 1
 1046 by 1.5 degree grid. White regions indicate non-significant regression estimates at the 99%
 1047 confidence level. QBO10 and QBO30 represent the QBO index at 10 and at 30 hPa, respectively.
 1048 The coefficients are in DU per unit change of corresponding normalized explanatory variable.
 1049 Note the different color bar range for the alternative EESC variable (a range of -30 to 30 against -
 1050 10 to 10 for the other plots).

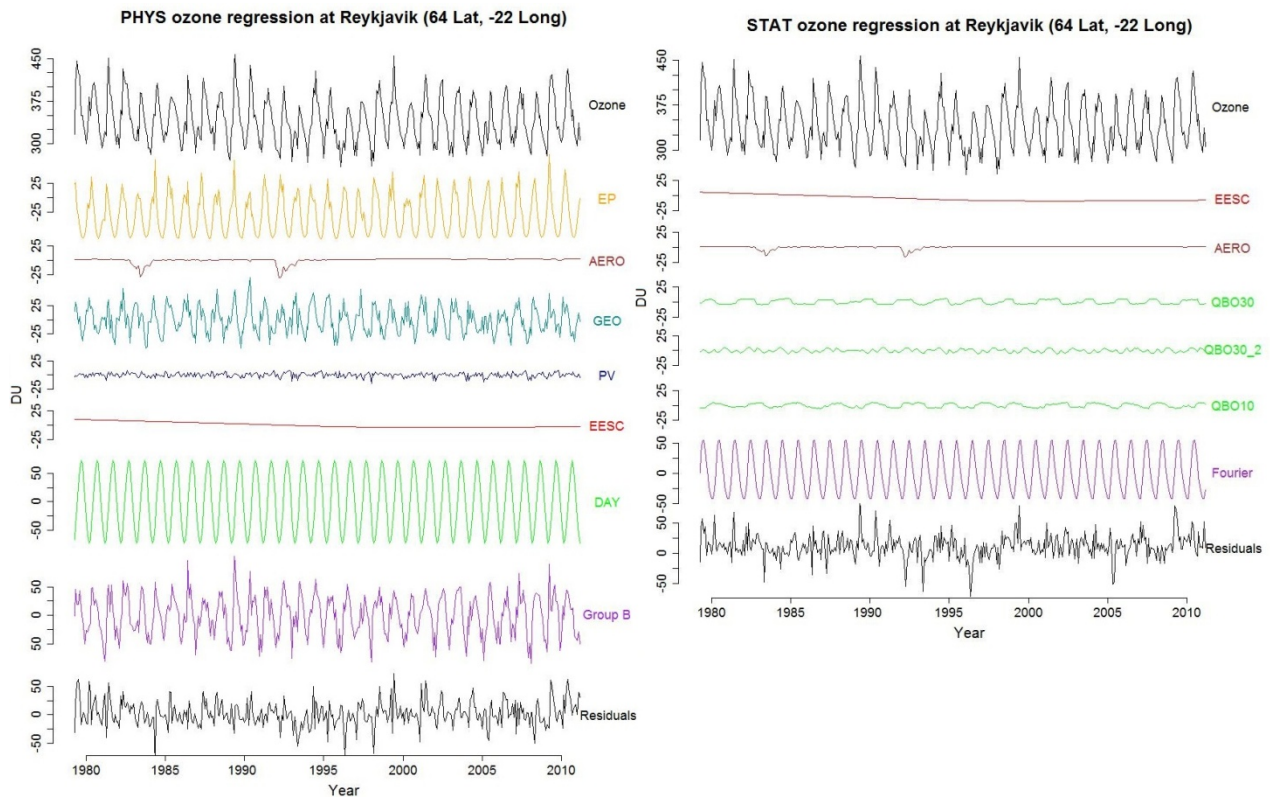


1051

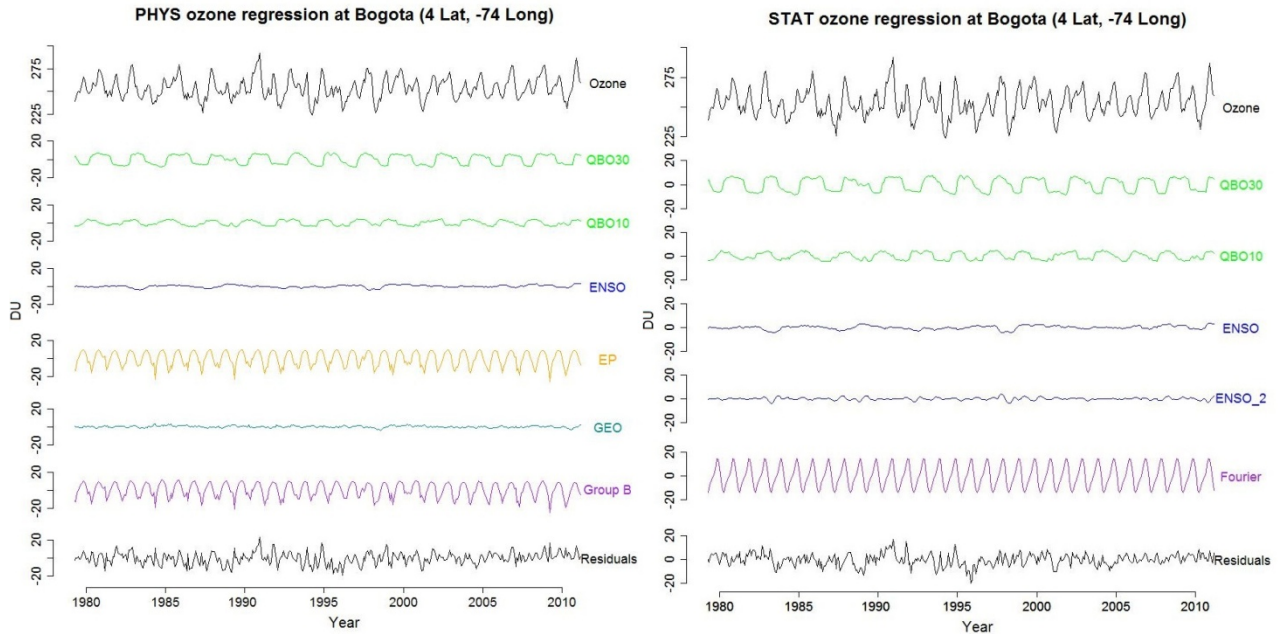
1052 **Figure 5.** Regression coefficient estimates of seasonal variables for the PHYS model on a 1 by 1.5
1053 degree grid. Note that south of 55°S in latitudes among the variables in group B only EP and PV
1054 are included to avoid correlation problems. The coefficients are in DU per unit change of
1055 corresponding normalized explanatory variable. White regions indicate non-significant regression
1056 estimates at the 99% confidence level.



1058 **Figure 6.** Regression coefficient estimates of non-seasonal variables for the STAT model on a 1
 1059 by 1.5 degree grid. White regions indicate non-significant regression estimates at the 99%
 1060 confidence level. QBO10 and QBO30 represent the QBO index at 10 and at 30 hPa, respectively.
 1061 The coefficients are in DU per unit change of corresponding normalized explanatory variable.
 1062 Note the different color bar range for the alternative EESC variable (a range of -30 to 30 against -
 1063 10 to 10 for the other plots).

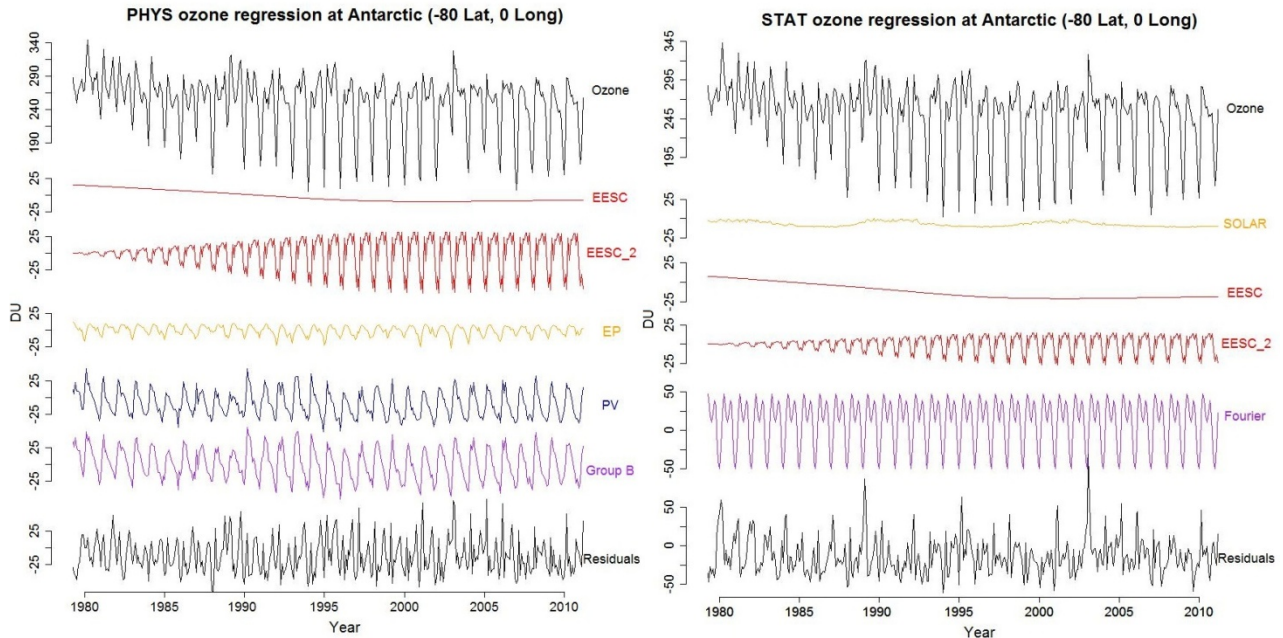


1064
 1065 **Figure 7.** Results of the PHYS regression (left plot) and of the STAT regression (right plot)
 1066 performed at Reykjavik, Iceland. “Fourier” is defined as the sum of the harmonic components that
 1067 describe seasonal variation in ozone and the “Group B” term is defined as the sum of EP, GEO,
 1068 PV and DAY, describing the seasonal component according to the PHYS model. QBO10 and
 1069 QBO30 index represent the QBO at 10 and at 30 hPa, respectively.



1070

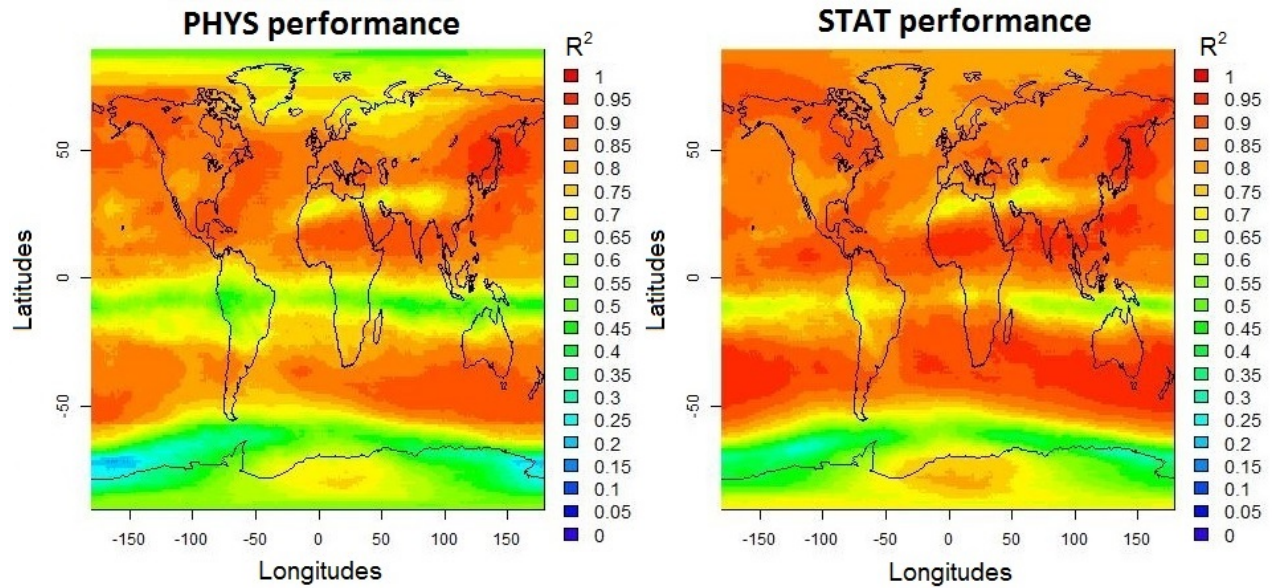
1071 **Figure 8.** Results of the PHYS regression (left plot) and of the STAT regression (right plot) at
 1072 Bogota, Colombia. “Fourier” is defined as the sum of the harmonic components that describe
 1073 seasonal variation in ozone and the “Group B” term is defined as the sum of EP and GEO,
 1074 describing the seasonal component according to the PHYS model. QBO10 and QBO30 represent
 1075 the QBO index at 10 and at 30 hPa, respectively.



1076

1077 **Figure 9.** Results of the PHYS regression (left plot) and of the STAT regression (right plot) at the
 1078 70°S, 0°E (Antarctica). “Fourier” is defined as the sum of the harmonic components that describe
 1079 seasonal variation in ozone and the “Group B” term is defined as the sum of EP and PV,
 1080 describing the seasonal component according to the PHYS model.

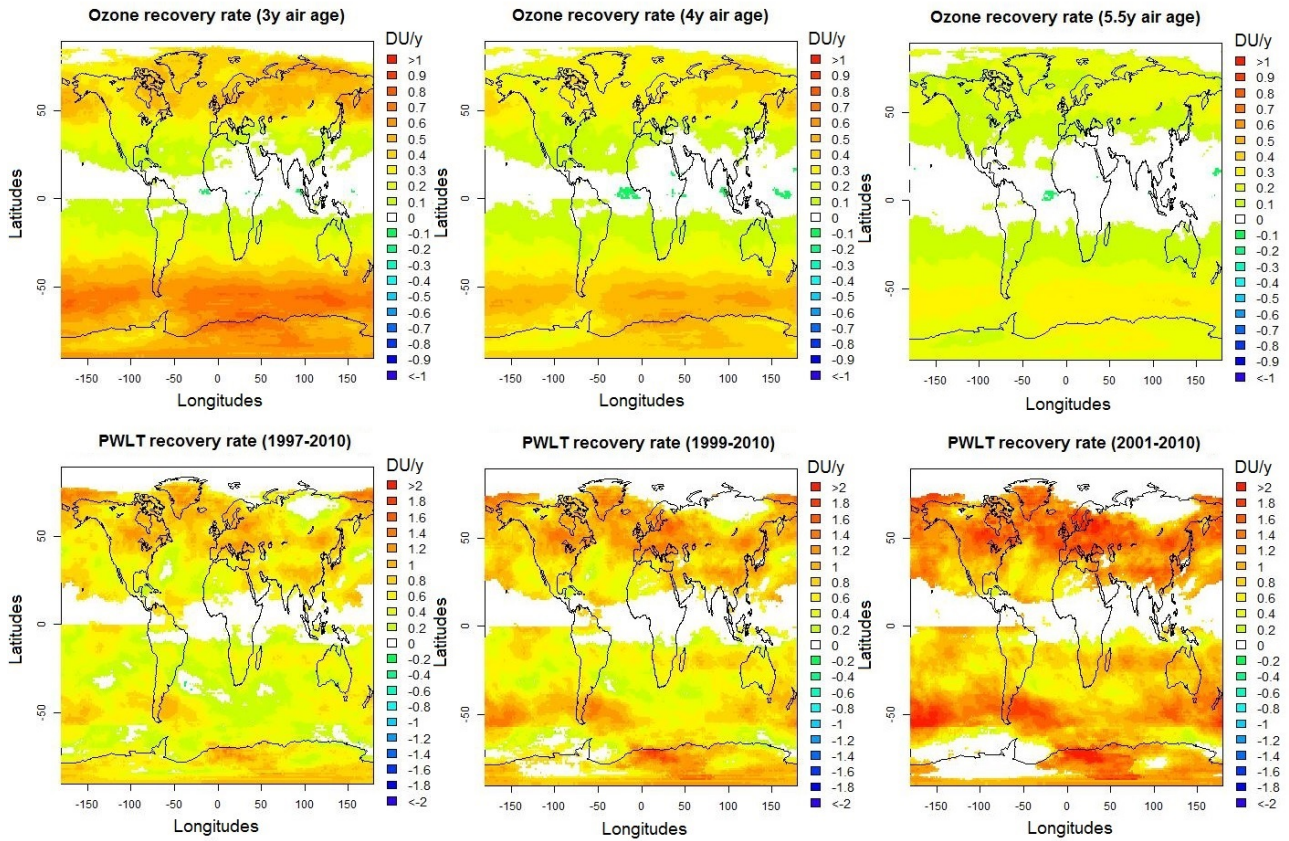
1081



1082

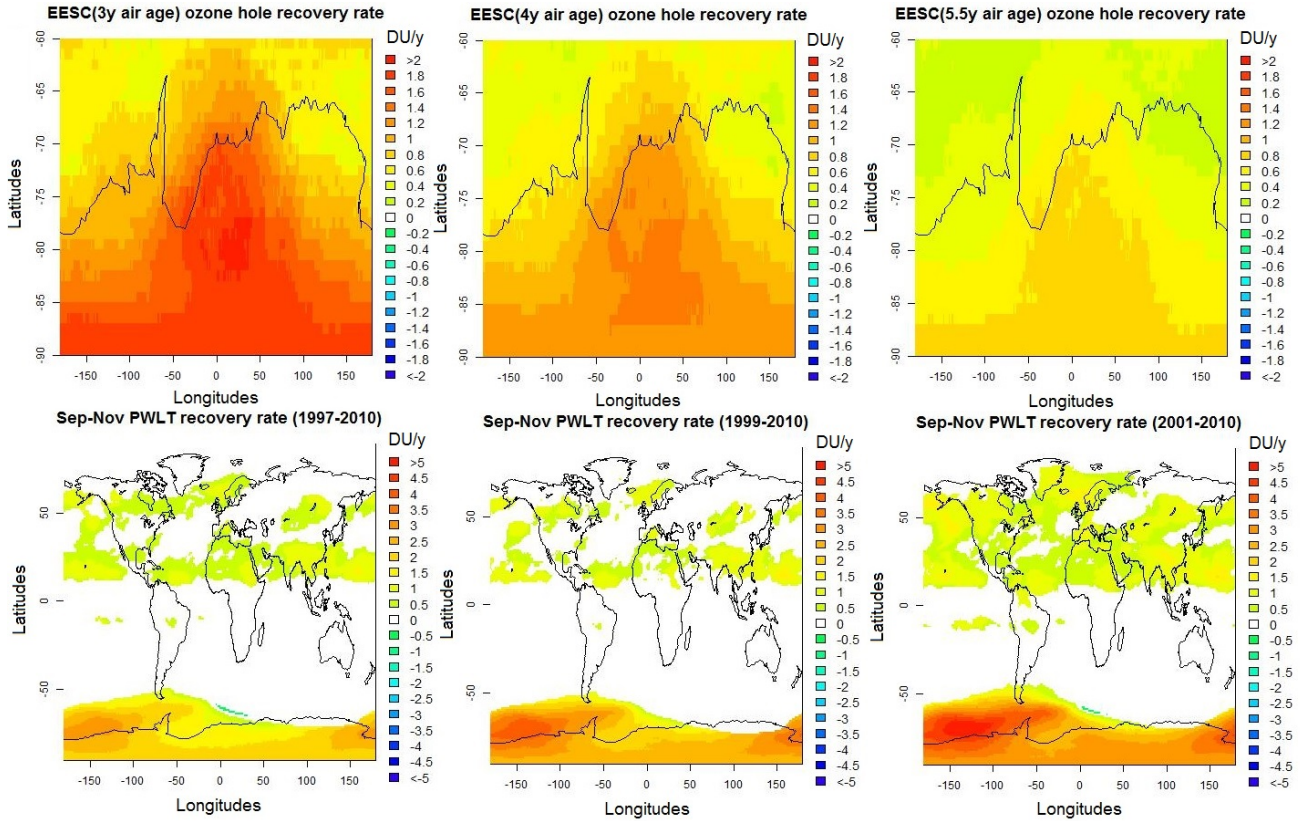
1083 **Figure 10.** The performance of the PHYS regressions (left plot) and STAT regressions (right plot)
1084 in terms of R^2 .

1085

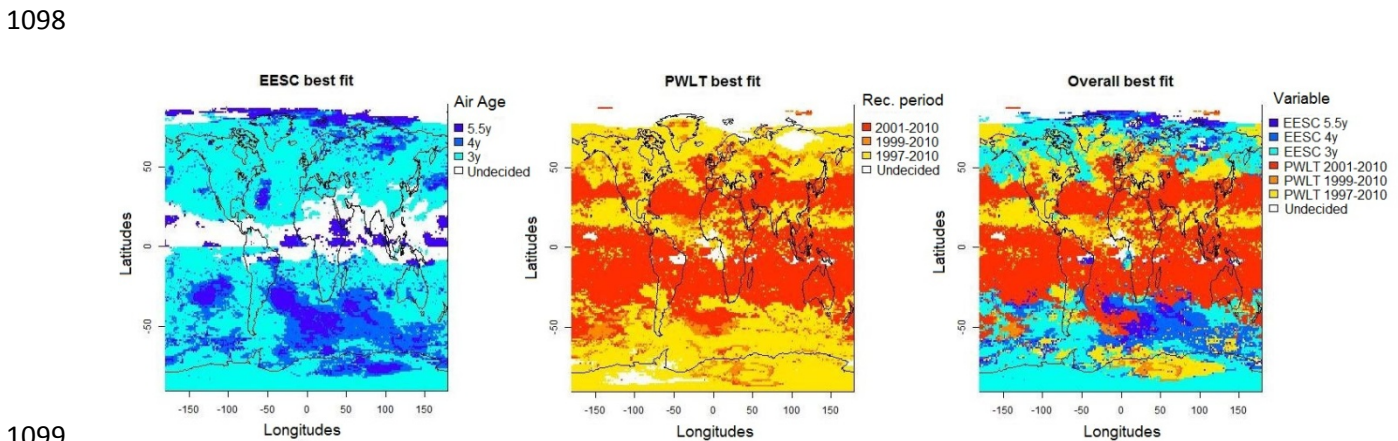


1086
1087 **Figure 11.** Ozone recovery rates based on EESC regression estimates (upper plots) or the
1088 piecewise linear function regression estimates (lower plots) using the PHYS model. Note that the
1089 color bar for the upper plots ranges from -1 to 1 DU/year, whereas for the lower plots the colorbar
1090 ranges from -2 to 2 DU/year.

1091



1092
 1093 **Figure 12.** Ozone recovery rates based on EESC and EESC_2 regression estimates for the PHYS
 1094 regressions south of 55°S (upper plots) and the straight forward piecewise linear regression
 1095 estimates (lower plots) on ozone data averaged over September - November months. Note that the
 1096 color bar for the upper plots ranges from -2 to 2 DU/year, whereas for the lower plots the colorbar
 1097 ranges from -5 to 5 DU/year.



1100 **Figure 13.** Comparison of R^2 values of PHYS regression runs depending on the parameterization
1101 for long term ozone variation by the EESC with air ages 3, 4 or 5.5 years or a piecewise linear
1102 function with the second linear component spanning 1997-2010, 1999-2010 or 2001-2010. The left
1103 plot illustrates which age of air parameter results in the highest R^2 value among the EESC
1104 parameterizations. The middle plot similarly illustrates which recovery period achieves the highest
1105 performance in terms of R^2 . The right plot shows result of similar comparisons among all
1106 parameterizations for long term ozone variation. White regions indicate non-significant regression
1107 estimates for each of the considered explanatory variables based on a 99% significance level.

1108

1109